Distributions of PGE and Re-Os isotope systematics in chromite from the Coobina chromitite deposit in Western Australia: Implications for chromite as a sulfide mineralisation indicator

*Louise Schoneveld[1]**, *Stephen Barnes[1]*, *Igor S. Puchtel[2]*, *Svetlana Tessalina[3]*,

Marek Locmelis[5]

[1]Discovery, Mineral Resources, CSIRO, Kensington, Western Australia, Australia

[2]Department of Geology, University of Maryland, College Park, MD 20742, USA

[3]John de Laeter Centre,Curtin University, Kent St Bentley 6102 WA[5]Department of Geosciences and Geological and Petroleum Engineering, Missouri University of Science & Technology, Rolla, Missouri, USA

*Corresponding author: louise.schoneveld@csiro.au

Revised for *Canadian Mineralogist*

Version 2022-07-05

Abstract

The abundance of Ru in chromite has been suggested as an indicator of sulfide liquid saturation in komatiites. The komatiite magma-derived Archean Coobina intrusion is known to be barren in terms of sulfide mineralization. Therefore, the Coobina intrusion allows for a useful case study to test the applicability of Ru abundance in chromite as a potential indicator for sulfide mineralization, as well as for better understanding the PGE-chromite association in general.

The Coobina intrusion is a highly deformed layered intrusion, interpreted as a flared dyke. It contains multiple massive chromitite seams that have been recently mined for metallurgical grade chromite. In this study, 18 samples from chromitite seams throughout this intrusion are investigated for their whole-rock platinum-group element (PGE) contents which is compared to their chromite mineral chemistry; including PGE content, platinum-group mineral (PGM) mineralogy, and Re-Os isotope systematics. Each sample has a similar chromite major and minor element chemistry, but a unique trace element signature, even within the same seam. In general, there are higher concentrations of Ru (>300 ppb) within chromite in the south-east, (toward the feeder dyke) and lower concentrations (<50 ppb Ru) in the north-west. At a sample scale, Ru in the whole rock and Ru in solid solution in the chromite are inversely correlated, while Ir shows a positive correlation between the whole rock and chromite mineral chemistry, indicating differing partitioning behaviours within the Iridium-group PGE (IPGE = Os, Ir, Ru). The inverse correlation between Ru in solid solution within chromite and Ru in whole-rock chromitite suggests that, for seams with high Ru in whole rock, Ru is occurring within separate PGM phases. This is supported by the observation that the samples with high whole rock Ru also have a high number of visible metal alloy and/or PGM inclusions. Although these inclusions are not necessarily Ru-rich phases, their presence suggests that there is a preference for these samples to form nuggets, which may restrict Ru partitioning into the chromite crystal structure. We suggest that the low Ru values in the Coobina chromite are a result of transient sulfide saturation.

If using chromite as a detrital indicator mineral for magmatic sulfide exploration, it must be kept in mind that transient sulfide saturation within chromitite seams may give a false positive signature.

Introduction

Chromite has been associated with economically viable concentrations of platinum group elements (PGE), particularly the more chromite-compatible iridium-subgroup PGE (IPGE = Ir, Ru, Os) and Rh, in locations such as the Merensky Reef of the Bushveld Complex of South Africa (Barnes *et al.* 2004, Smith *et al.* 2021). The part that chromite plays in this PGE accumulation has been the subject of numerous studies (Teigler & Eales 1993, Godel *et al.* 2007). Since the advent of laser ablation ICP-MS and its application to analysis of trace elements at sub-ppm level, it has been possible to investigate to what extent IPGE in chromite-rich rocks are present in solid solution in the chromite lattice, as opposed to occurring as discrete IPGE-rich minerals (Locmelis *et al.* 2011, Pagé *et al.* 2012, Park *et al.* 2017). The IPGE contents of chromite and chromite-rich rocks have been used as a constraint in petrogenetic models (Finnigan *et al.* 2008, Naldrett *et al.* 2009a, Park *et al.* 2012, Prichard *et al.* 2017) and provenance studies (Pagé & Barnes 2009, González-Jiménez *et al.* 2015, Pagé & Barnes 2016). In the case of extrusive komatiites, it has been shown that concentrations of IPGE in chromite can exceed hundreds of ppb (Locmelis *et al.* 2011). Fiorentini *et al.* (2004) found that IPGE predominantly occur as micro-inclusions in chromite within komatiitic basalts, but are present in solid solution in chromite within true komatiites. Locmelis and co-authors (Locmelis *et al.* 2011, Locmelis *et al.* 2013, Locmelis *et al.* 2018) proposed that chromite lattice Ru concentration of less than 150 ppb has the potential to indicate equilibration with sulfide liquid and therefore, chromite may be a useful mineral indicator in exploration for magmatic sulfide ores. However, Pagé and Barnes (2016) found that IPGE in chromite tend to be present at much lower concentrations in intrusive rocks relative to extrusive rocks formed from the equivalent magma types, which suggests that intrusive-hosted chromite could represent a false positive signal for this exploration indicator if analysed in soils/surface samples or ex-situ from their host rock.

The Coobina chromite deposit in the Archean Sylvania Inlier in Western Australia (Figure 1) is a rare example of an intrusive layered body of komatiitic affinity, containing thick chromitite seams, for which a large amount of whole-rock PGE data is already available (Barnes & Jones 2013). It provides an opportunity to investigate the distribution of IPGE hosted in solid solution in the chromite lattice versus the presence of discrete platinum group minerals (PGM) in samples with no known association with magmatic sulfides. Therefore, a detailed study of the IPGE contents in the Coobina intrusion will provide novel information useful for provenance studies and allow to further evaluate the relationship between Ru in chromite and the presence or absence of magmatic sulfides. In addition, Re-Os isotope data for the Coobina chromitites provide a new data point on the Archean mantle isotope evolution curve for Os, as well as help decipher the source of PGE in these chromitites.

The Coobina chromitites have been previously investigated by Barnes and Jones (2013) focussing on the structure of the strongly folded and sheared seams. These authors found that the chromite major element chemistry is indicative of a komatiitic origin and the crystal size distribution is suggestive of in-situ growth rather than mechanical sorting. The chromitite whole-rock PGE contents are low, with values of ~100 ppb for Ru and Ir. The Mg/Fe ratios of chromite within the chromitite seams may have been re-equilibrated with the olivine cumulates they are hosted within. Extensive shearing and folding due to the Capricorn orogen makes it difficult to trace the seams between pits, either by structural or even chemical measurements.

In this study we build on the work by Barnes and Jones (2013) and we further investigate the chemistry of chromite using LA-ICP-MS. Eighteen chromitite samples were analysed for trace elements and integrated with the whole-rock and chromite major element data of Barnes and Jones (2013) to infer the controls on the trace element incorporation into chromite and PGM nugget formation. Three chromitite samples, including one replicate, were also investigated for their Re-Os isotope systematics and Re and PGE abundances. A particular area of interest is the partitioning behaviour of Ru, as Ru content of chromite has been proposed to be a potential indicator for sulfide saturation in komatiite magmas and, hence, for magmatic Ni-sulfide prospectivity (Locmelis *et al.* 2011, Locmelis *et al.* 2013, Locmelis *et al.* 2018).

Geological setting

The Coobina chromitite mine is located ~50 km southeast of Newman (Figure 1), within the Archean Sylvania Inlier in the southern Pilbara Craton of Western Australia. The Coobina mine was owned and mined as a ferrochrome resource by Consolidated Minerals Ltd. from 2002 through 2013.

The chromite ore is hosted by a large ultramafic cumulate body, which intruded along the SE contact between the Jimblebar Greenstone Belt and foliated granite of the Sylvania Inlier (Williams & Tyler 1991). The current outcrop at Coobina represents a vertical section (younging to the NW) through an Archean ultramafic intrusion with an interpreted 10 km long feeder conduit toward the east (Figure 1) (Tyler 1991). An anorthositic metagabbro to leucogabbro is found along the northern part of the ultramafic body, in places with a gradational contact. The intrusion is strongly deformed through a series of major east-west trending shears that extended through the region, likely related to the early Proterozoic Capricorn Orogeny associated with the collision of the southern Pilbara and northern Yilgarn Cratons at c. 1830-1780 Ma (Cawood & Tyler 2004, Occhipinti *et al.* 2004).

Apart from a broad Archean classification for the Coobina intrusion, no reliable age information is available. Uranium-Pb zircon data available from the Geological Survey of Western Australia GeoView database on the overlying Jimblebar Belt greenstones comprise two dates of 3.193 and 3.185 Ga from felsic metavolcanic rocks (Wingate *et al.* 2019b, a) and maximum deposition ages of 3.565-3.573 Ga for metasedimentary units within the belt. One date of 3.185 Ga from a felsic intrusive rock within the outcrop area of the Coobina intrusion is also available, which can be taken as a minimum age for the intrusion itself. The intrusion, therefore, can be bracketed to have been emplaced between 3.193 and 3.185 Ga. Tyler (1991) suggest that the Inlier forms a separate micro-terrane of meso-Archean age that amalgamated with the main Pilbara Craton between 2.76 and 3.00 Ga.

The Coobina intrusion is made up of a serpentinite (formerly dunitic) body, several hundreds of metres thick, which hosts a series of chromite lenses and an underlying peridotite-dominated unit. The intrusion has undergone multiple phases of deformation to the point where the chromitite seams are isoclinally folded, making it difficult to assess whether they were uniformly distributed through the dunite section pre-deformation, but the outcrop distribution suggests that there were probably two main intervals with thick chromitite lenses towards the top of the dunite unit (Fig. 1).

Abundant sub-parallel chromite lenses are observed throughout the serpentinite and range from 2 cm to 2 m in width and up to 350 m in length (Figure 2). Primary layering (mm-cm scale) is only observed within and near the chromite lenses. The boundaries of the chromite lenses vary from sharp to diffuse, with massive chromite-rich (~85% chromite) lenses commonly grading into zones of disseminated chromite. The lenticular form of the chromitite bodies is considered to be the result of boudinage developed during extensive tight and locally isoclinal folding of originally laterally continuous seams (Barnes & Jones 2013).

The field relationships are consistent with the Coobina intrusion being a composite ultramafic-mafic layered intrusion with Great Dyke-like flared dyke geometry and internal magmatic differentiation. Chemically, the high MgO content of the cumulates and the compositions of the chromites (Cr/[Cr+Al] = 0.7 - 0.85, MgO/[MgO+FeO] = 0.30 - 0.55 and low Fe^{3+} contents) indicate a likely Al-undepleted komatiitic parental magma (Barnes and Jones 2013).

Samples

There are a total of 150 samples that were originally analysed using electron microprobe and 46 of these were analysed for whole rock PGE content in the Barnes and Jones (2014) study. In the study covered here, 18 samples with varying whole-rock PGE content were chosen for trace element and isotopic analysis. The sample names and locations are summarised in Figure 1 and Table 1. The samples were taken from the chromite seams and consist of primary euhedral chromite (Figure 3) with minor interstitial serpentine (likely after olivine). The samples were mounted in epoxy and fashioned into 25 mm diameter polished rounds for microanalysis.

Three samples (BC1, NC2 and WS2) from seams within different pits were analysed in detail for their texture (Figure 4). These three samples were chosen based on their spatial location and on their whole-rock Ru abundances giving a range of 70 ppb, 87 ppb and 174 ppb Ru, respectively. These 3 samples, along with an additional sample (NS3 – 115 ppb Ru) were also examined for their visible inclusion populations and PGE mineralogy. Two samples from the Coobina intrusion were also analysed for the Re-Os isotope systematics.

Analytical techniques

This study integrates electron microprobe data from Barnes and Jones (2013) with new chromite trace element data obtained on 18 samples via LA ICP-MS. Our study also uses the new data on the PGE content within the chromite to compare with the whole-rock PGE contents published in the Barnes and Jones (2013) study. Additionally, new Re-Os isotopic and Re and PGE abundance data were obtained for 2 samples (and one replicate) of chromitite via negative thermal ionization mass-spectrometry (N-TIMS) and Isotope Dilution Multi-Collector Inductively-Couple Plasma Mass Spectrometry (ID MC-ICP-MS), following the methods described below. Detailed methods for the whole-rock analysis and major element analysis of chromite are detailed in Barnes and Jones (2013). Therefore, only a short summary is presented here.

Whole-rock elemental abundances, including the PGE (Ir, Ru, Rh, Pt, and Pd), were measured on 2 kg aliquots from 46 samples (with 4 replicates) at GeoScience laboratories (Ontario Geological Survey, Sudbury, Canada) using a specially customized method of sodium metaphosphate fluxed nickel sulfide fire assay preconcentration followed by ICP-MS (Bédard & Barnes 2004). Of these samples, 41 were also analysed for whole-rock major element concentrations. The results from these analyses were included within the Barnes and Jones (2013) study, and are revisited here to give context to the trace element abundances measured within the chromite grains.

The major element analysis of 150 samples of chromitite were conducted using a Cameca SX50 electron microprobe at CSIRO-ARRC (Australian Resources Research Centre; Kensington, Western Australia) using standard wavelength-dispersive spectrometry, 30-nA beam current, 15 kV accelerating voltage, and 100 s counting times. The analysis targeted centres of unaltered grains, away from cracks, with 8-12 points analyzed per sample. All data are available for download from the supplementary material in the Barnes and Jones (2013) study. The ferric iron content of each analysis was estimated in this study by the Barnes (1998) method; i.e. assuming stoichiometry, and an ideal XY_2O_4 where X = (Fe^{2+}, Ni, Mn, Co, Zn) and Y = (Cr^{3+},Fe^{3+}, Al). Titanium was assumed to be present as an ulvöspinel component, and V is assigned to a fictive component. Iron is subdivided into ferrous and ferric to satisfy the conditions $n_y = 2n_x$ where n_y is the total number of atoms of trivalent cations and n_x is the total moles of divalent cations per unit cell.

Os isotopic, Re and PGE bulk chromitite abundance data.

The analytical protocols used in this study to obtain the Re-Os isotopic and Re and PGE abundance data for the chromite samples followed those described in detail by (Puchtel *et al.* 2014) and Puchtel *et al.* . The analyses were performed at the Isotope Geochemistry Laboratory (IGL), University of Maryland, College Park, USA. In summary, 0.015-0.057 g of crushed, unground whole-rock chromitite sample, 5 mL of double Os-purged, triple-distilled concentrated HNO_3, 4 mL of triple-distilled concentrated HCl, and appropriate amounts of mixed ^{185}Re-^{190}Os and PGE (^{99}Ru,^{105}Pd,^{191}Ir,^{194}Pt) spikes were sealed in double, internally-cleaned, chilled 25 mL Pyrex™ borosilicate Carius Tubes and heated to 270°C for 96 h. Osmium was extracted from the acid solution by CCl_4 solvent extraction (Cohen & Waters 1996), then back-extracted into HBr, followed by purification via microdistillation (Birck *et al.* 1997). Ruthenium, Pd, Re, Ir, and Pt were separated and purified using anion exchange chromatography following the protocol of (Rehkämper & Halliday 1997) with some modifications. Average total analytical blanks (TAB) during the analytical campaign were (in pg): Re 0.33 ± 0.07, Os 0.40 ± 0.14, Ir 0.43 ± 0.26, Ru 3.3 ± 3.2, Pt 5.1 ± 2.8, and Pd 3.3 ± 1.9 (± 2SE, N = 3). For the three chromite samples analysed, the total analytical blanks for Os, Ir, and Ru constitute less than 0.07% of the total element analysed. Blank contributions for Re varied between 9% and 19%, for Pt – between 1.5% and 4.9%, and for Pd – between 4.1% and 5.3% of the total element analysed.

Osmium isotopic measurements were accomplished via negative thermal ionization mass-spectrometry (N-TIMS: (Creaser *et al.* 1991). All samples were analysed using a secondary electron multiplier (SEM) detector of a *ThermoFisher Triton*® mass spectrometer at the IGL. The measured isotopic ratios were corrected for mass fractionation using $^{192}Os/^{188}Os = 3.083$. The internal precision of measured $^{187}Os/^{188}Os$ ratios in all three samples was 0.05-0.06% relative (2SE). The $^{187}Os/^{188}Os$ of 300 pg loads of the in-house Johnson-Matthey Os standard measured over the period of 2 years leading up to the current analytical session averaged 0.11376 ± 11 (± 2SD, N = 54). This value characterizes the external precision of the Os isotopic analysis (0.10%) and represents the true uncertainty on the measured $^{187}Os/^{188}Os$ ratio for each individual sample. The $^{187}Os/^{188}Os$ ratio measured in each sample was also corrected for the instrumental bias relative to the average $^{187}Os/^{188}Os = 0.11378$ precisely measured in the Johnson-Matthey Os standard on the Faraday cups of the IGL Triton (Puchtel *et al.* 2014).

The measurements of Ru, Pd, Re, Ir, and Pt were performed at the IGL via inductively coupled plasma mass-spectrometry (ICP-MS) using a *Nu Plasma* instrument with a triple electron multiplier configuration in a static mode. Isotopic mass fractionation was monitored and corrected for by interspersal of samples with standards. The accuracy of the data was assessed by comparing the results for the reference materials UB-N and GP-13 obtained during the ongoing analytical campaign. Concentrations of all HSE and Os isotopic compositions obtained at the IGL are in good agreement with the results from other laboratories (Table 1 in Puchtel *et al.* (2014)). Diluted spiked aliquots of iron meteorites were run during each analytical session as secondary standards. The results from these runs agreed within 1% for Re and Ir, and within 2% for Ru, Pt, and Pd, with fractionation-corrected values obtained from measurements of undiluted iron meteorite solutions using Faraday cups of the same instrument with signals of >100 mV for the minor isotopes. We, therefore, cite 0.1% as uncertainty on the concentration of Os, ±1% on the concentrations of Ir, and ±2% relative on the concentrations of Ru in the three samples analysed. The uncertainties on the

Re concentrations were between 4.6 and 9.6%, Pt – between 2.0 and 2.4%, and Pd – between 2.1 and 2.6% relative, assuming a ~50% variation in the Re and PGE abundances in the average TAB. The uncertainty on the Re concentration was the main source of uncertainty on the Re/Os ratio. For the three samples analysed, this uncertainty was estimated to be between 4.7 and 9.7% relative.

The initial γ^{187}Os values were calculated as per cent deviation of the isotopic composition at 3.2 Ga (the accepted age of the Coobina intrusion) relative to the chondritic reference of (Shirey & Walker 1998) at that time. The average chondritic Os isotopic composition at 3.2 Ga was calculated using the ^{187}Re decay constant $\lambda = 1.666 \times 10^{-11}$ year^{-1} (Smoliar *et al.* 1996) and an early Solar System initial ^{187}Os/^{188}Os = 0.09531 at 4.58 Ga and ^{187}Re/^{188}Os = 0.40186 (Smoliar *et al.* 1996, Shirey & Walker 1998).

Trace elements in chromite

Eighteen chromitite samples were selected for trace element analysis to represent the variable range of PGE in the whole-rock samples. 10-12 150 µm diameter ablations were carried out on each sample for a total of 225 chromite trace element analyses. These analysis were conducted using a Photonmachines, ATLex 300si-x Excite 193nm Excimer ArF laser attached to an Agilent 7700 ICP-MS in the National Geosequestration Laboratory, CSIRO, Kensington, Western Australia. The ablation was set 3 J/cm^2 fluence at a rate of 9 Hz. The plasma conditions were optimized daily, to obtain highest counts with oxide production, with ^{248}ThO/^{232}Th remaining below 0.4%.

Isotopes measured in this study were: ^{27}Al, ^{29}Si, ^{47}Ti, ^{51}V, ^{53}Cr, ^{55}Mn, ^{59}Co, ^{60,61,62,64}Ni, ^{63,65}Cu, ^{66}Zn, ^{99,100,101,102,104}Ru, ^{103}Rh, ^{105,106,108}Pd, ^{107}Ag, ^{111}Cd, ^{191,193}Ir, ^{192}Os, ^{194,195}Pt, ^{197}Au. Reference materials USGS GSD-2g, a basaltic glass doped with trace elements, and UQAC-FeS-1 (developed by Universite du Quebec a Chicoutimi), a Ni-Cu-Fe-S pressed power doped with trace elements, were used as bracketing standards during data reduction. UQAC-FeS-1 was used as the primary reference material for the PGEs and precious metals while GSD-2g was used as the bracketing standard for all other elements. Fe^{57} was used as the internal standard, using average values of Fe in chromite measured by electron microprobe for individual chromitite samples (and given in Barnes and Jones, 2013). The relative standard deviation of Fe wt.% in each sample ranges from 2% up to 15%.

The USGS-MASS-1 and UQAC-FeS-5 reference materials were used to assess the precision and accuracy of the laser ablation ICP-MS analysis. The measured values of these standards are generally within 10% relative to the published values and have a precision within 6% (1SD). Details of the secondary standard analysis are included in the supplementary material. Time resolved analysis was undertaken with 30 seconds of background with the laser off, then 260 laser pulses were collected which is approximately ~30 seconds of signal. The data was reduced using Iolite v.3.63 (Paton *et al.* 2011), choosing an integration window that avoids any large spikes in the time resolved analysis that would indicate a sub-surface micro-nugget effect. There was a delay of 20 sec. between different analyses to allow for sufficient washout of the signal. The average detection limits for the PGEs in chromite from this method are < 10 ppb (see supplementary material).

Two samples were also analysed by LA-ICP-MS mapping to investigate trace element and PGM distributions in larger areas. The method for this analysis type is included in the supplementary material. Some chromite analyses were duplicated at CCFS/GEMOC, Macquarie University, Sydney, Australia using a Photon Machines Excite Excimer laser ablation system connected to an Agilent 7700cx ICP-MS and give very similar results using Al^{27} as the internal standard and PGE-A (Alard *et al.* 2000) and NIST610 (Norman *et al.* 1996) as bracketing standards. Details for these analyses are included within the supplementary material.

Results

Textures

The crystal size distribution (CSD) was quantified by measuring individual chromite grain areas on back-scattered electron images using Fiji (Schindelin *et al.* 2012) following the method outlined by Higgins (2000) and Higgins (2006). CSDs are expressed as number densities of grains per unit area per unit length of bin size and are used to understand the number of crystal growth populations or possibly grain resorption or post-cumulous re-crystallisation. CSDs were measured on three samples, that vary significantly in their whole rock PGE content to determine if crystallisation history may play a role in the distribution of the PGE content.

Sample BC1 has a measured whole-rock PGE content of 70 ppb and was located in the Blatchfords Main pit. This sample shows a slight reduction in the amount of small grains which suggests some coarsening or sintering (post-cumulus recrystallisation) has occurred in this sample. Sample NC2 from the Newlands Creek pit has a whole rock Ru value of 87 ppb while WS2 from Wrights South pit has a Ru value of 174 ppb. Although these two samples have very different Ru whole rock contents, they show almost identical crystal size distribution patterns.

Major and trace element analysis of chromite

The major element chemistry of chromite within the Coobina chromitite was discussed in detail by Barnes and Jones (2013). The chromite major element chemistry is broadly similar throughout the entire deposit (Figure 5) and similar to other chromitites worldwide (Barnes and Roeder, 2001). Barnes and Jones (2013) suggested that the chromite within the Coobina deposit has undergone metamorphic exchange of Mg and Fe with the spatially associated olivine based on linear relationships between Mg# (molar Mg/(Mg+Fe^{2+}) and Cr# (molar Cr/(Cr+Al)) within individual seams. This chemical exchange gives rise to a relatively greater Fe enrichment in samples with lower modal abundance of chromite, but no evidence was found for significant modification of the proportions of the major trivalent components Cr, Al and Fe^{3+} (Fig. 3A) in these chromites. The proportions of the trivalent cations show some overlap with the field for layered intrusions (Barnes & Roeder 2001), but with its unusually Cr-rich character, the Coobina chromite data array fits more closely to chromite compositions from Al-undepleted komatiites (Barnes 1998). If this chromite were sampled as a resistant indicator mineral, it would be impossible to determine the provenance by major element chemistry alone.

The chromite species throughout the Coobina intrusion show minor variations of Cr# between 0.6 and 0.9 and Mg# between 0.2 and 0.6, but on the scale of individual samples, they have previously been shown to display an inverse correlation (*cf.*, Barnes and Jones, 2013). The new LA ICP-MS data reported here show that Ti, V, Zn, and Co are positively correlated with the Cr# of the chromite, while Ni shows a weak negative correlation (Figure 6A-E).

New data are presented here for the IPGE and the PPGE chemistry of chromite. The average PGE contents in chromite for each sample show a weak negative correlation of Ir with Cr# (Figure 6G-L), but no other detectable correlation of PGEs with the Cr or Fe^{3+} content (supplementary material Figure 15). Os and Ir concentrations in chromite are positively correlated, ranging from below the detection limit of <10 ppb up to ~100 ppb (Figure 7). Concentrations of Ru and Rh are also strongly correlated (Pagé *et al.* 2012, Park *et al.* 2017), although the concentrations for Ru that are almost one order of magnitude higher than for Rh. Palladium and Os show no correlation with Ru, while Pt contents are mostly below the detection limit in chromite (i.e., <6 ppb). The distribution of Ru in these chromites is not correlated with any of the key major element ratios (Figure 6, supplementary Figure 15). The Ru contents in chromite can be separated into 2 groups, those with and average Ru in chromite of >160 ppb (6 samples) and those with <90 ppb (12 samples). In general, chromite with the highest Ru concentrations is located closest to the contact of the chromitite-free peridotite and closer to the suspected feeder dyke of the intrusion (Figure 8) while the lower Ru in chromite values are located closer to the upper contact with the overlying leucogabbro. However, there is significant deformation, folding, and shearing of the chromitite seams, which makes tracing individual seams on a scale greater than a few hundred metres difficult (Figure 8).

Whole rock PGE analysis

The whole rock chromitite PGE abundance data presented by Barnes and Jones (2013) are compared to and integrated with the new in-situ PGE analysis of chromite to better understand the distribution of these elements on the mineral, sample, and intrusion scales. As illustrated in Figure 9E-F, primitive mantle (PM) normalized PGE patterns are overall similar between the chromite and whole-rock chromitite samples. However, while Ru displays a relatively narrow range in whole rock analysis of 47-174 ppb Ru between 46 samples, Ru contents in chromite vary between 10 and 314 ppb across all chromite grains analysed. Platinum contents in chromite are at or below the detection limit of ~6 ppb Pt, whereas Pt in the whole rock chromitite samples is highly variable, with contents between 3 and 64 ppb.

Investigating three replicates of the whole-rock analyses from Barnes and Jones (2013), Ru, Rh, and Pd standard deviations between replicates are between 0.1 and 8% relative of the measured value. Pt variability is much larger with the three replicates having variances between 25 and 62% relative of their measure value (13-51 ppb Pt). One sample (with low whole-rock Pt abundance of 2.6 ppb) has a variance of only 3%. This shows that the Pt abundances may not be reproducible with the whole-rock analysis methodology used due to the tendency of Pt to form nuggets.

Presence of nuggets and inclusions of other phases

We analysed the visible nugget/inclusion populations of 4 samples (BC1, NC2, NS3 and WS2) that represent the two distinct groups; samples of high Ru in chromite and low bulk rock values and vice versa (Figure 10). The whole-rock chromitite PGE contents are not directly reflected by the chromite-lattice bound PGE contents, which suggest the presence of

PGE-bearing phases as small inclusions which we investigated using high resolution back-scattered electron (BSE) images that show representative inclusions. These images are included as supplementary material. Due to the small size (<4 μm) of the inclusions and the fast scan EDS technique used, only the major element components can be determined from these inclusions and not the full mineral chemistry. Also, it should be noted that the inclusions observed represent the visible size fraction of the inclusions, and it is possible that much smaller (nm) inclusions exists within these samples.

Most of the visible inclusions are near the edge of the grains or within crystal voids (Figure 12). There is no clear correlation between size and type of inclusions and the degree of sintering (post-cumulus recrystallisation) indicated by crystal size distributions (Figure 4). Sample BC1 represents low Ru abundance in the whole-rock (70 ppb) and high values of Ru within chromite (218 ppb). This sample has 11 visible phases that are considered "bright phases" in SEM images, i.e., phases that contain elements with masses much higher than chromium which generally indicates the presence of native metals, sulfides, alloys, or PGMs. The small-sized (< 4 μm) inclusions (28% of the entire inclusion population) are composed mostly of Os-Ir-Pt minerals (Figure 12), but this sample also contains other phases, including sulfide, barite and Bi, Pb, and Sn-minerals. Similarly, sample NC2, which has comparable Ru abundances (87 ppb in the whole-rock, and 282 ppb within chromite) contains only 14 visible inclusions, most of which are less than 5μm in diameter and are dominated by PGMs (Figure 10).

Sample NS3 represents high Ru in the whole-rock (115 ppb) and low Ru within chromite (84 ppb). This sample has 30 visible bright inclusions that are all less than 4 μm (Figure 10). The inclusions are composed of Os-Ir-Ru phases (Figure 10), but this sample also contains phases such as native gold, barite and Bi- and W minerals. Sample WS2 has 44 bright inclusions, all of which were identified as galena (PbS) by rapid EDS analysis. However, a PGM inclusion was found during LA-ICP-MS mapping (Figure 12), along with many small regions with very high Pb concentrations. This rock has the lowest Ru abundance within the chromite (21 ppb), while the whole rock Ru abundance is high (174 ppb). Of these 4 samples examined for bright phases and inclusions, the samples with the highest whole rock Ru values have the largest number of inclusions.

Re-Os isotopic data and Re and PGE abundances in chromitites

Three chromitite samples, including one replicate (Chr1_1, Chr1_2, and Chr2), were analysed for their Re-Os isotopic compositions and Re and PGE abundances (Table 2). The chromitites have low Re abundances, ranging from 0.062 to 0.11 ppb, and relatively high Os concentrations, between 38 and 408 ppb, resulting in very low Re/Os ratios and, thus, minimal age corrections for the radioactive decay of ^{187}Re. The initial γ^{187}Os values of the three samples calculated for the age of the Jimblebar greenstone belt and Coobina ultramafic rock emplacement of ~3.189 Ga (the average age obtained using U-Pb zircon dating of the surrounding felsic rocks) vary in a narrow range between -0.53±0.10 and -0.74±0.10, indicating evolution of the mantle source of the Coobina intrusion mafic-ultramafic rocks with a long-term near-chondritic ^{187}Re/^{188}Os ratio. Because of the very narrow range of variations in the ^{187}Re/^{188}Os ratios between the three chromitites analysed, no reliable isochron can be obtained using these data.

Although Pt and Pd abundances are relatively constant and low in the three samples, Os, Ir, and Ru are high and quite variable (Table 2), even between the two separately processed aliquots of the same whole-rock sample (Chr1), indicating non-uniform distribution of Os-Ir alloy and possibly laurite (RuS_2) inclusions within the chromitite or highly localised PGE variations within a sample.

Chromite contribution to the whole rock chromitite PGE content

We calculated the proportion of chromite in the Coobina chromitites after Pagé and Barnes (2016) using Eq. (1):

$$\% \, Cr - Spinel \; in \; sample = F^{Cr-Spinel} = {Cr_2O_3}^{WR} \Big/ {Cr_2O_3}^{Cr-Spinel} \qquad (1)$$

Where $Cr_2O_3^{WR}$ and $Cr_2O_3^{Cr\text{-}Spinel}$ are the Cr content in the whole rock (WR) and chromite in wt. % oxide, respectively. The values of the chromite contribution to the chromitites ranges from 61 to 78% in the Coobina samples, similar to those calculated for the chromitites analysed by Pagé and Barnes (2016) of 40% - 87%. Equation (1) assumes that all chromium in the whole-rock is contained within the chromite, which will results in a slight overestimation, as olivine, the dominant mineral in komatiites, can contain up to ~2000 ppm Cr (Pagé *et al.* 2012, Locmelis *et al.* 2019). Using the value calculated using equation (1), we can calculate the proportion of the PGE in the whole rock that are incorporated in the chromite:

$$F_i^{Cr-Spinel} = \left(C_i^{Cr-Spinel} * F_i^{Cr-Spinel}\right) / C_i^{WR} \quad (2)$$

Where *i* is the PGE of interest and C is the concentration in ppb. Equation 2 assumes that all PGE and Cr are contained in the chromite.

Using the PGE contents shown in Table 3, it is evident that the whole-rock budget and chromite chemistry show some discrepancies, as evidenced by the >200% of the PGE being attributed to chromite, which results in a negative value for C_{Ru}^{melt}. Consequently, the Ru abundances in individual grains cannot represent the entire inventory in the whole rock analysis.

Discussion

Understanding what controls the PGE budget of chromite has implications for the use of chromite as an indicator mineral in exploration for nickel sulfide ores in komatiites (e.g., Locmelis *et al.* (2018)) and for the use of chromite chemistry in petrogenetic studies ((Finnigan *et al.* 2008, Naldrett *et al.* 2009a, Park *et al.* 2012, Prichard *et al.* 2017).

Re-Os isotope systematics of the Coobina komatiite source

Apart from the “broadly Archean” age, based mainly on field relationships and U-Th dating of surrounding units, there is no direct age determinations for the Coobina layered intrusion. However, the U-Pb zircon ages of 3.193 and 3.185 Ga (the average age is 3.189 Ga) for the felsic volcanic rocks associated with the Coobina intrusion (Wingate *et al.* 2019b, a) provide an indirect constraint on the age of the intrusion.

Although no reliable Re-Os isochron can be obtained for the Coobina ultramafic intrusion, Re-Os model ages can be calculated for each of the three chromitite samples. These calculated model ages, termed T_{MA} and T_{RD} (Shirey and Walker, 1998), are reported in Table 2. Time of separation from mantle that is growing according to chondritic evolution is represented by T_{MA}. It is calculated by assuming that the Re/Os of the sample is representative of its long-term history in the mantle. The time of Re depletion (T_{RD}) age is the minimum age for Re depletion. It is calculated assuming that a melt-depletion event previously removed all Re from the sample, and hence, growth of ^{187}Os was completely terminated at that time. Because the chromitites have very low, magmatic Re abundances, apparently not disturbed since the time of the emplacement of the intrusion, the calculated T_{MA} model ages (average $T_{MA} = 3.28 \pm 0.03$ Ga) are very similar to the T_{RD} model ages (average T_{RD} = 3.25±0.08 Ga). These Re-Os model ages are in good agreement with the bracketed age of the Coobina intrusion of between 3.193 and 3.185 Ga .

As is evident from Table 2, the analyzed samples are characterized by relatively large variations in Os abundances, indicating presence of Os-rich nuggets in the chromitite. However, such sample heterogeneity does not have an adverse effect on the calculated initial Os isotopic composition as long as the mineral phases analyzed represent primary, magmatic phases. This condition is obviously met for the Coobina chromitite, where the chromite represents a magmatic phase that crystallized from the parental komatiite magma.

Using the accepted emplacement age of 3.189 Ga and the average initial Os isotopic composition of the three chromitites (γ^{187}Os(3.189 Ga) = –0.63±0.21), the long-term Re/Os ratio with which the source of the Coobina parental komatiite magma evolved can be estimated. In order to model the time-integrated evolution of Re/Os in the Coobina mantle source, the average initial ^{187}Os/^{188}Os ratio obtained for the Coobina chromitites (0.10442±22) has been used to calculate the minimum ^{187}Re/^{188}Os ratio required to evolve to this Os isotopic composition by 3.189 Ga, and assuming formation of this mantle domain shortly after the start of the Solar System. Evolution of the Coobina komatiite source from an early Solar System ^{187}Os/^{188}Os = 0.09531 at 4558 Ma (Smoliar *et al.* 1996, Shirey & Walker 1998) to the initial ^{187}Os/^{188}Os ratio of 0.10442±22 at 3.189 Ga requires ^{187}Re/^{188}Os ratio of 0.375±9. This time-integrated ^{187}Re/^{188}Os ratio for the Coobina komatiite system is within the range of chondritic meteorites (a bulk chondrite average ^{187}Re/^{188}Os = 0.410±51 (±2SD), as compiled from the data of Walker *et al.* , Brandon *et al.* , and Fischer-Gödde *et al.* , and its calculated γ^{187}Os(3.189 Ga) value of –0.63±0.21 is also within the range of most Archean and Proterozoic komatiite sources (Figure 10), albeit on the lower end of the range. It is also identical to the γ^{187}Os(3.18 Ga) value of –0.38±0.43 obtained by Puchtel *et al.* for the contemporaneous Ruth Well komatiites from the Pilbara Craton, whose source was calculated to have evolved with time-integrated ^{187}Re/^{188}Os = 0.385 ± 18 and was interpreted by Puchtel et al. (2022) to be derived from the convecting upper mantle. In summary, the Re-Os isotopic composition of the Coobina chromitite is consistent with derivation of the Coobina parental komatiite magma from the convecting upper mantle source, providing evidence for the mantle origin of the Coobina PGE inventory.

Trace elements in chromite

The commonly measured trace elements in chromite (Zn, V, Mn, Ti, Co) are positively correlated with Cr#. The Cr# is least likely to be altered by postmagmatic processes (Barnes, 2000) and, thus, interpreted to reflect primary magmatic processes. Nickel is not correlated with Cr#, averaging 510 ± 100 ppm throughout all measured samples. As the dominate silicate phase within the chromitite seams is olivine, this consistent Ni value may be due to equilibration with olivine. Comparing the Coobina Ni values to chromite from other komatiitic parent bodies (Figure 13), these Ni contents are low, similar to those measured for komatiites that experienced sulfide saturation and removal of immiscible sulfide liquid (Locmelis *et al.* 2018).

Righter *et al.* (2004) and Brenan *et al.* (2012) showed that Ru is compatible within chromite, and that the $D_{(spinel/melt)}$ value is a strong function of the redox state of the system. This arises from two factors: (1) Ru^{2+} is less soluble in silicate melt than Ru^{3+} (Borisov & Nachtweyh 1998, Brenan *et al.* 2012) and (2) Ru^{3+} has an increasing affinity for more Fe^{3+} rich spinels owing to the shared oxidation state and its octahedral site preference. Therefore, precipitation of discrete Ru phases observed in the Coobina chromitite may be due to reduction of Ru^{3+} to Ru^{2+} over the solubility line (Finnigan *et al.* 2008). Ru^{2+} is the dominant Ru species in silicate melts under highly reduced conditions (in equilibrium with graphite). The Coobina chromitite samples show that Rh concentration is highly correlated with Ru suggesting the possibility that both are existing as dominantly divalent cations.

Chromite at Coobina is generally low in ferric iron, with the Fe^{3+}/trivalent cation ratio averaging 0.08 ± 0.04, typical of komatiites, which are generally regarded as having crystallised near the FMQ buffer (Canil & O'Neill 1996), although some evidence exists for a more reduced early Archean mantle recorded by komatiites (Locmelis *et al.* 2019, Nicklas *et al.* 2019).

Chromite in chromitites: partitioning and parental melts

Ruthenium is compatible in chromite; however, the published partition coefficients vary widely. Experimental measurements by Brenan *et al.* (2012) at 1400˚C and under redox conditions of ΔIW+7.2 (calc. ΔFQM +3.74) gives D_{Ru} of 38, with a predicted value of ~30 in typical ferric iron-poor chromite. Studies by Righter *et al.* (2004) produced extremely high partition coefficients, with D_{Ru} >1000 at 1300˚C and log fO_2 -5.07 (calc. ΔFQM +2.15), while Pagé *et al.* (2012) calculated partitioning of the PGE into chromite from natural komatiites at

$D^{(chromite/melt)}$ values around 79 for Ru and 9.5 for Ir. Park *et al.* (2012) found that D_{Ru} is dependent on oxygen fugacity, with oxidising environments increasing the partition coefficient of Ru and the other PGE significantly. The latter study showed, in agreement with Pagé *et al.* (2012), that IPGE contents of chromite in intrusive settings are much less than those in volcanic rocks of probably similar magmatic affinity. This implies that cooling rate may play an important role in the final redistribution of Ru, the most likely mechanism being solid state diffusive equilibration with Iridium-group platinum group mineral (IPGM) phases.

To evaluate the contribution of chromite to the whole-rock PGE budget, the rocks were normalised to 100% chromite (see Equation 2 and Table 3), removing the small contribution of the olivine (now serpentine) component. These results suggest that the whole rock samples were made of ~60-80% chromite. This calculation, however, assumes that the PGE abundances within the chromite throughout the large (>2kg) sample were homogeneously distributed and/or were accurately represented by a small subsample analysed by LA-ICP-MS. We can see in Table 3 that this is not the case, as when the Ru content in the chromite is high, the chromite makes up >200% of the whole rock PGE budget. This suggests that the high-Ru chromite may be extremely localised, either due to local changes in the chromite partition coefficients and/or a gradual reduction of Ru^{3+} to Ru^{2+} in the melt over time which decreased its compatibility in chromite. When comparing these results with other layered intrusions (Figure 14), such as the Great Dyke, Bushveld, and Black Thor (Pagé & Barnes 2016), Ru abundances in chromite and in whole rock samples are characterized by a weak negative correlation. Notably, the Great Dyke is also calculated to have more than 100% contributions of the PGE to the whole rock concentration (Pagé and Barnes, 2016) from chromite suggesting that either the proportion of chromite is underestimated or the partitioning of Ru into chromite is overestimated in these samples. The concentration of the PGE in the equilibrium/parent melt can also be calculated using partition coefficients.

Fiorentini *et al.* (2008) compared whole rock Ru abundances in 2.7 Ga mineralised and unmineralized komatiites. The whole-rock analysis of barren samples shows a strong correlation between Cr (ppm) and Ru (ppb), where the Ru contents range from 2 ppb to 10 ppb (Fiorentini *et al.* 2008). The mineralised komatiites have no strong correlation between Ru and Cr, with Ru values between 1 and 20 ppb. Older (3.5–3.2 Ga) barren komattites generally have lower values of all the PGEs including Ru, which have measured values of 2-5 ppb Ru (Maier *et al.* 2009). Using the partitioning coefficient of D_{Ru} = 79 (Page et al., 2012), the calculated silicate component in equilibrium with the Coobina chromite would have a Ru value of between 5-24 ppb. It has been found that intrusive samples tend to have lower partitioning of the PGEs than their extrusive counterparts, suggesting these partition coefficients may be on the higher end of the range. These values are in reasonable agreement with those for barren komatiites from ~3.2 Ga.

The general trend of these chromite seams is an inverse correlation between Ru in chromite and the Ru in the whole rock (Figure 9B). As these rocks are chromitites, lacking any evidence for a magmatic sulfide component, the implication is that the Ru in the more Ru-rich samples occurs within separate PGM phases, and that the abundance of these phases is in inverse proportion to the concentration of Ru in the chromite lattice. This is supported by the evidence that samples with high whole rock Ru also have high abundances of PGMs and alloys. The presence of discrete IPGE inclusions suggests that there is a preference for Ru in these samples to form micro-nuggets, rather than partitioning into the chromite lattice such as observed in the NS3 sample Figure 10C and supplementary images.

Metals, nuggets and inclusions.

A common issue in interpreting PGE signatures is the tendency of PGE to form discrete phases (nuggets), i.e. PGMs (Cabri *et al.* 1996, Park *et al.* 2012, Barnes *et al.* 2021). The nugget effect can cause issues in bulk analysis from measuring nuggets that are unevenly distributed at the scale of the analytical aliquot, which can cause large standard deviations in replicate analysis (Barnes *et al.* 2021), as in the Pt analysis presented here.

However, it is noted that replicates measured in this study did not show a large variation in Ru abundances, which may reflect that the inclusions, measured in this study, average approximately 4 µm in the longest direction. Micro-nuggets, such as these, can be accounted for by the whole rock analysis, but tend to be missed during LA ICP-MS microanalysis. These micro-inclusions are of various phases, such as galena, PGMs, native gold, and alloys, and are most frequently found within the outer rims of chromite grains (Figure 12) or within voids. In their experiments, Brenan *et al.* (2012) and Finnigan *et al.* (2008) observed the tendency for small alloy and sulfide grains to nucleate on the chromite-melt interface. This is also observed in natural systems, such as the Bushveld Complex, where the chromite and PGM are closely spatially associated (Naldrett *et al.* 2009a).

Ruthenium as an indicator of sulfide saturation in komatiitic chromite

Within a small range of major element chromite compositions, we observe two populations, both >160 ppb Ru and much lower than 100 ppb Ru within the chromite. These populations are similar to the <150 ppb Ru value, which is thought to indicate sulfide saturation in komatiitic systems (Barnes & Fiorentini 2008, Locmelis *et al.* 2018). The major element chemistry of the Coobina chromites are almost indistinguishable to those of known komatiitic basalt parentage, and the trace element chemistry shows both depleted Ni and depleted Ru signatures which could be interpreted to reflect derivation from a sulfide-saturated komatiite magma as proposed by Locmelis et al. (2018). However, sulfides are absent in the exposed portion of the intrusion and have not been found despite extensive mining and exploration efforts. Therefore, the low Ru in chromite will yield a false positive result if used as a detrital indicator mineral (i.e., without outcrop context) in the exploration for magmatic Ni-Cu sulfide deposits. The false positive may be related to the intrusive nature of the Coobina body and/or the age of the intrusion. Pagé and Barnes (2016) suggest that due to the long cooling times in chromitites in intrusions, the chromites can recrystalise resulting in reequilibration of the PGE which can diffuse into sulfide phases. However, based on the very similar crystal size distribution (CSD) measurements between all samples (Figure 4), the low-Ru chromite is not correlated to extensive recrystallisation/sintering, which would produce CSDs with a reduction in the small sizes and a flattening of the CSD slope (such as shown in Hunt *et al.* (2021)), suggesting that these changes are not due to local recrystalisation and subsequent redistrubution of these elements. Furthermore, Ru is extremely difficult to remobilize (Locmelis *et al.* 2010). Also contributing to the low Ru in chromite signal is the age of these intrusions as older komatiitic bodies have measured Ru values that are lower than the 2.7 Ga komatiites used for the indicator study. If chromite are to be used as a prospectivity indicator for sulfide, without the context of age, low Ru value may be interpreted as a false positive signature for sulfide saturation.

The key observation in this data set is the decoupling between the whole-rock Ru abundance and Ru content in chromite. The observed inverse correlation implies that there is an independent control on the whole rock content of Ru in the more Ru-enriched samples, and that this control is accompanied by depletion of Ru hosted in solid solution of the chromite lattice. One possibility is that the Ru-enriched (in whole rock) samples owe their chemistry to accumulation of Ru-enriched PGMs, such as alloys or laurite, from IPGE-saturated melt (Barnes & Fiorentini 2008). However, if this was the case, then the parental magma to both the PGM phases and the chromite must have been saturated in Ru-rich PGM, and hence the chromite should have an Ru content proportionate to saturation levels of Ru. It should, therefore, be enriched in Ru, not depleted relative to chromite that formed from Ru-undersaturated magma.

A hint to a possible control may lie in the IPGE-enriched chromitites of the Harold's Grave locality in the Shetland Ophiolite (Prichard *et al.* 2017). In this unusual chromitite occurrence, whole-rock enrichments up to several ppm of IPGE, with only minor Pt and Pd and exceptionally high Ir/Pd ratios of around 50, are associated with large (100-2000 μm) interstitial aggregates of IPGM and minor sulfides between chromite grains. This mode of occurrence is in marked contrast to the typical occurrence of IPGMs in chromitites as inclusions within chromite grains. Prichard *et al.* (2017) postulated that these aggregates were the remnants of partially remelted sulfide droplets generated by transient sulfide saturation during chromite accumulation. As the sulfide droplets remelted, their IPGE contents increased to levels of hundreds of ppm at which point they became saturated in IPGM, which were left behind as the remainder of the sulfide subsequently redissolved. The process is analogous to that proposed by Fonseca *et al.* (2012) to account for growth of IPGM phases during mantle partial melting, and the Shetland chromitites are indeed mantle rocks. The result is a rock with high IPGE contents and little or no sulfide. This process has been invoked by Barnes *et al.* (2021) as a general explanation for the PGE-chromitite association in layered intrusions, accounting for the entire spectrum from low-S IPGE-enriched chromitite to sulfide-bearing chromitite hosted PGE reefs, such as the UG2 chromitite layer of the Bushveld Complex. Furthermore, within the Merensky Reef of the Bushveld Complex, a depletion of PGE contents is observed further from the feeder dyke (Naldrett *et al.* 2009b) attributed to the deposition of sulfide closest to the feeder structures. This is the opposite to what is observed at Coobina, where the whole rock values of Ru apparently decrease (and while the Ru in chromite increase) toward the feeder dyke (Figure 8), suggesting the generation of immiscible sulfide liquid is taking place far from the feeder, while the chromite close to the feeder have higher Ru in chromite values, not affected by the far field transient sulfide saturation, though due to the heavily folded nature of the Coobina seams, it is difficult to determine if this is a true spatial association.

Transient sulfide saturation could explain elevated whole-rock Ru (along with Ir and Os) in the more enriched Coobina samples. This would also provide an explanation for the Ru depletion of the chromite in the same rock. Competition for IPGE between sulfide and chromite results in depletion of the chromite in Ru, as observed in komatiitic chromite associated with magmatic sulfide mineralisation (Locmelis *et al.* 2013, Locmelis *et al.* 2018). A recent study by Hunt *et al.* (2021) suggests it is possible (and common) for chromite seams to remain permeable to fresh melt derived from the overlying magma. This would allow fresh melt to percolate through and redissolve any precipitated sulfide. Transient sulfide saturation during the chromite formation and subsequent re-dissolution of the sulfide and re-distribution through percolating melt would provide an explanation for the seemingly paradoxical binary distribution of relatively Ru rich chromitite with Ru poor chromite on one hand, and Ru-poor chromitite with the very localised relatively Ru-rich chromite on the other.

Implications for the Ru in chromite mineral indicator

If the explanation proposed here is correct, then Ru in chromite in the particular case of chromitite seams is highly susceptible to even at grain scale, transient style sulfide saturation. If sampled in an indicator mineral campaign, chromite grains derived from such an environment would give a false positive result for the exploration of magmatic Ni-Cu-PGE sulfides.

Even so, as these chromites are from plutonic settings, they have a high proportion of very coarse grains while as extrusive settings tend to have much smaller grains. Prospective regions could potentially be identified by a combination of chromite grain size and chemistry, along with the integration of additional exploration proxies, such as Ni and Cu in olivine (Locmelis *et al.* 2019, Barnes *et al.* in press), the trace element content of arsenides (Le Vaillant *et al.* 2018), and zoning pattern in pyroxene (Schoneveld *et al.* 2020). Furthermore, chromitite is an extremely rare rock type, even within large ultramafic-dominated intrusions, so its contribution to regional sample populations is likely to be small compared with chromite derived from much more voluminous rocks containing disseminated chromite.

Regardless, given the increased demand for battery metals for the green energy transition, the presence of a false positive leading to continued exploration may be more desirable than a false negative, where a potential resource is missed entirely.

Conclusions

The Coobina Intrusion is a derivation of a komatiite magma from a convecting upper mantle source that evolved with long-term near-chondritic ^{187}Re/^{188}Os ratio. The calculated average Re-Os model ages for the chromitites, T_{MA} = 3.28±0.03 Ga and T_{RD} = 3.25±0.08 Ga, are consistent with the accepted emplacement age of the Coobina intrusion at 3.189 Ga.

Chromite in the Coobina Intrusion shows a wide variability in its Ru content, which shows an inverse relationship with the Ru content in whole-rock. There are two possible explanations for this phenomenon:

1) The Ru partition coefficient for chromite is locally lowered via changes in redox conditions, transient sulfide accumulation or a combination of both. The system reaches saturation in Ru-rich PGMs to form micron-scale nuggets that precipitate as a cumulus phase. These cumulate PGMs settle into the lower regions, increasing the Ru content in a rock containing previously crystalised low-Ru chromite.

2) The high Ru rocks were formed under conditions of transient sulfide saturation during chromite growth, increasing the whole-rock Ru content, but lowering the Ru content in solid solution in chromite. The sulfide phases then re-dissolve during late-stage melt percolation and are re-distributed as PGMs. This process is envisaged as being similar to that responsible for anomalously high IPGE concentrations in some unusual ophiolitic chromitites and is related more generally to the global PGE-chromite-sulfide association.

The ratio of Ru between chromite in solid solution and whole-rock chromitite is not correlated with any crystal chemical component. This favours the transient sulfide saturation mechanism rather than a change in oxidation state, which would be evident in the major element composition of the chromite, particularly its trivalent cation (i.e., Fe^{3+}, Al^{3+}, Cr^{3+}) content. Furthermore, as there is no textural evidence of recrystallisation in the studied samples, the process of recrystallisation and redistribution during slow cooling does not appear to have played a major role.

Although this intrusion was mined for many years for its chromium resource, there has been no sulfide observed within this intrusion. The chromite within the Coobina intrusions has Ru in solid solution of values of both >150 ppb Ru and < 150 ppb Ru. As low (<150 ppb) Ru content in komatiitic derived chromite has been suggested to indicate sulfide saturation, we suggest that the Coobina intrusion has undergone transient sulfide saturation at small scale. When using chromite as a detrital indicator mineral for the exploration for nickel sulfide, the possibility of transient sulfide saturation should be considered and may indicate a false positive result.

Tables

Table 1: Chromitite samples analysed for PGE and trace elements within Chromite with reference to the pits outlined in Figure 1

Seam	Locality group	Trend-Area	Pit	Easting	Northing
4R	Blatchfords-C5	East	Blatchfords	222015.5	7399163
BM1	Blatchfords-C5	East	Blatchfords Main	222067	7399188
BM2	Blatchfords-C5	East	Blatchfords Main	222059	7399199
BC1	Blatchfords-C5	East	Blatchfords Main	222088	7399339
4K	Blatchfords-C5	East	Central Five	221804.6	7399051
2Q	Falcon-Skywest	Central	Falcon	221432	7399240
SW1	Falcon-Skywest	Central	Sky West	221547	7399402
1G	Finucane	West	Wrights	221218.6	7399865
1T	Finucane East	Central	Finucane	221491.6	7399871
FT3	Finucane East	Central	Finucane East	221540	7399843
NF2	Newlands 246	West	Newlands Four Pit	220945	7399305
NS3	Newlands 246	West	Newlands Six Pit	220945	7399102
3F	Newlands Ck	West	Newlands	221209	7399188
NC2	Newlands Ck	West	Newlands Creek Pit	221085	7398970
NE1	North Eastern Pits	NorthEast	North Eastern Pits	222097	7400448
5B	Tish-Wedgetail	East	Tish Creek	221798.5	7399345
WS2	Wrights	West	Wrights South Pit	221344	7399699
WS4	Wrights	West	Wrights South Pit	221344	7399699

Table 2: Re-Os isotopic and Re and PGE abundance data (in ppb) for the Coobina chromites

Sample No.	**Chr1_1**	**Chr1_2**	**Chr2**
Re	0.06239	0.1134	0.06305
Os	408.2	152.4	38.16
Ir	217.0	111.1	46.45
Ru	830.2	312.3	188.1
Pt	6.939	6.916	4.073
Pd	1.464	5.330	1.105
^{187}Re/^{188}Os	0.00073±0.0004	0.00358±0.00035	0.00794±0.00037
^{187}Os/^{188}Os	0.10447±6	0.10450±6	0.10496±6
γ^{187}Os(T)	-0.63	-0.74	-0.53
T_{MA}, Ga	3.28	3.30	3.27
T_{RD}, Ga	3.27	3.27	3.20

Initial γ^{187}Os values were calculated at $T = 3.189$ Ga.

Table 3: Mass balance Calculations as given by $C_i^{(melt)}=C_i^{WR}-(C_i^{Cr\text{-}Spinel} \times F_i^{(Cr\text{-}Spinel)})$ (Pagé and Barnes, 2016). C_i^{WR} is the concentration of the PGE within the whole rock and $C_i^{Cr\text{-}Spinel}$ is the concentration of the PGE within the chromite lattice, $F_i^{(Cr\text{-}Spinel)}$ = % PGE from the whole rock accounted for by the chromite. $C_i^{(melt)}$ is the concentrations of the PGE within the non-chromite component of the rock

				% PGE from the whole rock accounted for by the chromite					
Seam	Ru ppb WR	Ru ppb Chr	% Cr-Spinel in sample	$F_{Ir}^{(Cr\text{-}Spinel)}$	$F_{Ru}^{(Cr\text{-}Spinel)}$	$F_{Rh}^{(Cr\text{-}Spinel)}$	$C_{Ir}^{(melt)}$	$C_{Ru}^{(melt)}$	$C_{Rh}^{(melt)}$
BC1	70.24	227.84	**68%**	**61%**	**222%**	**225%**	**10.64**	**-85.35**	**-7.44**
BM1	73.1	240.85	78%	30%	257%	299%	29.88	-114.44	-13.89
NC2	86.96	244.16	**77%**	**48%**	**216%**	**61%**	**30.33**	**-100.93**	**11.31**
NS3	114.69	88.54	**76%**	**42%**	**59%**	**71%**	**30.77**	**47.05**	**4.31**
BM2	115.39	82.83	61%	28%	44%	78%	32.41	64.51	2.25
WS4	142.69	14.23	71%	22%	7%		30.65	132.61	
FT3	145.01	85.88	71%	39%	42%	59%	28.59	83.7	3.25
NF2	152.89	30.64	77%	18%	15%	18%	51.44	129.32	11.83
NE1	154.57	28.54	78%	53%	14%	10%	23.46	132.42	12.88
SW1	165.96	50.31	75%	29%	23%	14%	37.96	128.44	15.03
WS2	174.41	26.79	**78%**	**12%**	**12%**	**10%**	**60.46**	**153.47**	**11.65**

Figures

Figure 1: Location map – A) regional geology of the Sylvania Inlier and the Coobina Intrusion, modified from Williams and Tyler (1991), B) Local geology of the Jimblebar field area from GSWA online (1:250000 data set) with interpreted >10km long feeder dyke Williams and Tyler (1991). C) Detailed geological map showing the Coobina ultramafic sill with pit outlines, and Cr sample locations (from Barnes and Jones (2013)). With geological data from Jeffrey (2003; internal company report) and S. Jones. GDA1994 MGA Zone 51

Figure 2: A) Large northeast-trending chromite seams in Newlands Creek pit, B) finer scale layering of chromite seams in Falcon Pit C) folded chromite lenses from Newlands Pit. Images courtesy of (Barnes & Jones 2013)

Figure 3: Reflected light images of the samples in this study. LA-ICP-MS ablation craters visible in some samples (150µm diameter), line in bottom left of each images is 500um. See Table 1 for locations for each sample.

Figure 4: (A) crystal size distribution of chromite, EDS is Equivalent circle diameter in µm. (B to D) SEM images showing representative chromitite textures

Figure 5: EPMA data for Coobina (from Barnes and Jones (2013)), Bushveld, Great Dyke, Stillwater (Barnes and Roeder, 2001) and komatiitic chromite (Locmelis et al. (2018)) and fields of spinel compositions from layered intrusions – chromitites and Al-undepleted komatiites (AUDK) from Barnes & Roeder (2001)

Figure 6: Trace elements and platinum group elements against Cr/(Cr+Al). Shown are average EPMA and LA-ICP-MS analysis for each sample. The error is one standard deviation from analysis on multiple chromite grains in a single sample. Colour represents mine pit and shape differentiates seams within this pit

Figure 7: LA-ICP-MS analysis of PGE in chromite from the Coobina intrusion

Figure 8: Distribution of Ruthenium in Chromite. Higher concentrations (>300 ppb) in the south-east, toward the feeder dyke and low concentrations (< 50 ppb) in the north-west. Map modified from Barnes and Jones (2013). GDA1994 MGA Zone 51.

Figure 9: (A) Average LA-ICP-MS analysis of the PGE in chromite, compared to (B) Whole-rock PGE analysis of the corresponding samples described by Barnes and Jones (2013). Values in (A) and (B) are normalised to the composition of the primitive mantle (Palme & O'Neill 2014) and plotted with pyrolite (Williams et al. 2020). (C to F) Comparison of the whole rock PGE content with the chromite analysis for individual sample averages

Figure 10: Frequency and composition of chromite-hosted micro-nuggets in Coobina samples. Inclusion type given by EDS spectra for major content only

Figure 11: Initial ^{187}Os/^{188}Os isotopic compositions, expressed in γ^{187}Os terms, of the Archean and Proterozoic komatiite systems plotted as a function of age. The blue bar for the modern BSE estimate represents the 2SD of the mean from Meisel et al. (2001). The sources of the data are as follows. Lapland – Puchtel et al. (2020); Vetreny Belt – Puchtel et al. (2016b); Belingwe – Puchtel et al. (2009b); Boston Creek – Puchtel et al. (2018); Pyke Hill – Puchtel et al. (2004); Kostomuksha – Puchtel & Humayun (2005); Volotsk – Puchtel et al. (2007); Weltevreden and Komati – Puchtel et al. (2014); Schapenburg –Puchtel et al. (2009a), Puchtel et al. (2016a), Kelly, Ruth Well, and Regal – Puchtel et al. (2022), Coobina – this study. Uncertainties are 2SD. The Os isotopic data for chondritic meteorites are compiled from (Walker et al. 2002), (Brandon et al. 2005)), and (Fischer-Gödde et al. 2010) and are plotted as an envelope enclosed between the slanting purple lines and corresponding to the entire range of calculated modern γ^{187}Os values projected back to the Solar System initial ^{187}Os/^{188}Os ratio. All uncertainties are 2SD of the mean..

Figure 12: A-D) SEM images of bright phases within chromite E) Laser ablation maps (35um square laser spot) of sample WS2

Figure 13: Nickel content of chromite from the Coobina intrusion compared to data from Bushveld Complex (Park et al. 2012), komatiites, komatiitic basalts and ferropicrite (from Locmelis et al. 2018)

Figure 14: Ruthenium contents of chromitites and chromite from Coobina and comparison to stratiform chromitites and chromite from the Bushveld Complex, Stillwater, Great Dyke and Black Thor with data from Pagé and Barnes (2016).Whole Rock Ru values were calculated by the measured whole rock value divided by the proportion of chromite in the chromitite as shown in Table 3

Supplementary Figure

Figure 15: [Supplementary Figure] Trace elements against Fe3+/(Al+Cr+Fe3+) ratio. Average EPMA and LA-ICP-MS analysis for each sample. The error is one standard deviation from analysis on multiple chromite grains in a single sample. Colour represents locality and shape differentiates seams within this locality

References

ALARD, O., GRIFFIN, W.L., LORAND, J.P., JACKSON, S.E. & O'REILLY, S.Y. (2000) Non-chondritic distribution of the highly siderophile elements in mantle sulphides. *Nature* **407**, 891-894, https://doi.org/10.1038/35038049.

BARNES, S.-J., MAIER, W.D. & ASHWAL, L.D. (2004) Platinum-group element distribution in the Main Zone and Upper Zone of the Bushveld Complex, South Africa. *Chemical Geology* **208**, 293-317, https://doi.org/10.1016/j.chemgeo.2004.04.018.

BARNES, S., MAO, Y.-J., YAO, Z.-S., JESUS, A.B., YANG, S., TARANOVIC, V. & MAIER, W.D. (in press) Nickel in olivine as an exploration indicator for magmatic Ni-Cu sulfide deposits: a data review and re-evaluation. https://doi.org/10.2138/am-2022-8327, https://doi.org/10.2138/am-2022-8327.

BARNES, S.J. (1998) Chromite in Komatiites, I. Magmatic Controls on Crystallization and Composition. *Journal of Petrology* **39**, 32, https://doi.org/10.1093/petroj/39.10.1689.

BARNES, S.J. & ROEDER, P.L. (2001) The Range of Spinel Compositions in Terrestrial Mafic and Ultramafic Rocks. *Journal of Petrology* **42**, 24, https://doi.org/10.1093/petrology/42.12.2279.

BARNES, S.J. & FIORENTINI, M.L. (2008) Iridium, ruthenium and rhodium in komatiites: Evidence for iridium alloy saturation. *Chemical Geology* **257**, 44-58, https://doi.org/10.1016/j.chemgeo.2008.08.015.

BARNES, S.J. & JONES, S. (2013) Deformed Chromitite Layers in the Coobina Intrusion, Pilbara Craton, Western Australia*. *Economic Geology* **108**, 337-354, https://doi.org/10.2113/econgeo.108.2.337.

BARNES, S.J., RYAN, C., MOORHEAD, G., LATYPOV, R., MAIER, W.D., YUDOVSKAYA, M., GODEL, B., SCHONEVELD, L.E., LE VAILLANT, M. & PEARCE, M.B. (2021) Spatial association between platinum minerals and magmatic sulfides imaged with the Maia Mapper and implications for the origin of the chromite-sulfide-PGE association. *The Canadian Mineralogist* **59**, 1775-1799, https://doi.org/10.3749/canmin.2000100.

BÉDARD, L.P. & BARNES, S.-J. (2004) Improved Platinum-Group Element Extraction by NiS Fire Assay from Chromitite Ore Samples Using a Flux Containing Sodium Metaphosphate. **28**, 311-316, https://doi.org/10.1111/j.1751-908X.2004.tb00746.x.

BIRCK, J.L., BARMAN, M.R. & CAPMAS, F. (1997) Re-Os Isotopic Measurements at the Femtomole Level in Natural Samples. **21**, 19-27, https://doi.org/10.1111/j.1751-908X.1997.tb00528.x.

BORISOV, A.V. & NACHTWEYH, K. (1998) Ru Solubility in Silicate Melts: Experimental Results in Oxidizing Region. abstract no. 1320.

BRANDON, A.D., HUMAYUN, M., PUCHTEL, I.S. & ZOLENSKY, M.E. (2005) Re-Os isotopic systematics and platinum group element composition of the Tagish Lake carbonaceous chondrite. *Geochimica et Cosmochimica Acta* **69**, 1619-1631, https://doi.org/10.1016/j.gca.2004.10.005.

BRENAN, J.M., FINNIGAN, C.F., MCDONOUGH, W.F. & HOMOLOVA, V. (2012) Experimental constraints on the partitioning of Ru, Rh, Ir, Pt and Pd between chromite and silicate melt: The importance of ferric iron. *Chemical Geology* **302**, 16-32, https://doi.org/10.1016/j.chemgeo.2011.05.015.

CABRI, L., HARRIS, D.C. & WEISER, T. (1996) Mineralogy and distribution of platinum-group mineral (PGM) placer deposits of the world. *Exploration and Mining Geology* **5**, 73-167.

CANIL, D. & O'NEILL, H.S.C. (1996) Distribution of Ferric Iron in some Upper-Mantle Assemblages. *Journal of Petrology* **37**, 609-635, https://doi.org/10.1093/petrology/37.3.609.

CAWOOD, P.A. & TYLER, I.M. (2004) Assembling and reactivating the Proterozoic Capricorn Orogen: lithotectonic elements, orogenies, and significance. *Precambrian Research* **128**, 201-218, https://doi.org/10.1016/j.precamres.2003.09.001.

COHEN, A.S. & WATERS, F.G. (1996) Separation of osmium from geological materials by solvent extraction for analysis by thermal ionisation mass spectrometry. *Analytica Chimica Acta* **332**, 269-275, https://doi.org/10.1016/0003-2670(96)00226-7.

CREASER, R.A., PAPANASTASSIOU, D.A. & WASSERBURG, G.J. (1991) Negative thermal ion mass spectrometry of osmium, rhenium and iridium. *Geochimica et Cosmochimica Acta* **55**, 397-401, https://doi.org/10.1016/0016-7037(91)90427-7.

FINNIGAN, C.S., BRENAN, J.M., MUNGALL, J.E. & MCDONOUGH, W.F. (2008) Experiments and Models Bearing on the Role of Chromite as a Collector of Platinum Group Minerals by Local Reduction. *Journal of Petrology* **49**, 1647-1665, https://doi.org/10.1093/petrology/egn041.

FIORENTINI, M.L., STONE, W.E., BERESFORD, S.W. & BARLEY, M.E. (2004) Platinum-group element alloy inclusions in chromites from Archaean mafic-ultramafic units: evidence from the Abitibi and the Agnew-Wiluna Greenstone Belts. *Mineralogy and Petrology* **82**, 341-355, 10.1007/s00710-004-0044-6.

FIORENTINI, M.L., BERESFORD, S.W. & BARLEY, M.E. (2008) Ruthenium–chromium variation: a new lithogeochemical tool in the exploration for komatiite-hosted Ni—Cu–(PGE) deposits. *Economic geology and the bulletin of the Society of Economic Geologists* **103**, 431-437, http://dx.doi.org/10.2113/gsecongeo.103.2.431.

FISCHER-GÖDDE, M., BECKER, H. & WOMBACHER, F. (2010) Rhodium, gold and other highly siderophile element abundances in chondritic meteorites. *Geochimica et Cosmochimica Acta* **74**, 356-379, https://doi.org/10.1016/j.gca.2009.09.024.

FONSECA, R.O.C., LAURENZ, V., MALLMANN, G., LUGUET, A., HOEHNE, N. & JOCHUM, K.P. (2012) New constraints on the genesis and long-term stability of Os-rich alloys in the Earth's mantle. *Geochimica et Cosmochimica Acta* **87**, 227-242, https://doi.org/10.1016/j.gca.2012.04.002.

GODEL, B., BARNES, S.-J. & MAIER, W.D. (2007) Platinum-Group Elements in Sulphide Minerals, Platinum-Group Minerals, and Whole-Rocks of the Merensky Reef (Bushveld Complex, South Africa): Implications for the Formation of the Reef. *Journal of Petrology* **48**, 1569-1604, 10.1093/petrology/egm030 %J Journal of Petrology.

GONZÁLEZ-JIMÉNEZ, J.M., LOCMELIS, M., BELOUSOVA, E., GRIFFIN, W.L., GERVILLA, F., KERESTEDJIAN, T.N., O'REILLY, S.Y., PEARSON, N.J. & SERGEEVA, I. (2015) Genesis and tectonic implications of podiform chromitites in the metamorphosed ultramafic massif of Dobromirtsi (Bulgaria). *Gondwana Research* **27**, 555-574, https://doi.org/10.1016/j.gr.2013.09.020.

HIGGINS, M.D. (2000) Measurement of crystal size distribution. *American Mineralogist* **85**, 1105-1116.

HIGGINS, M.D. (2006) *Quantitative textural measurements in igneous and metamorphic petrology*. Cambridge University Press, Cambridge.

HUNT, E.J., O'DRISCOLL, B. & DAY, J.M.D. (2021) Sintering as a key process in the textural evolution of chromitite seams in layered mafic-ultramafic intrusions. *The Canadian Mineralogist* **59**, 1661-1692, 10.3749/canmin.2100021 %J The Canadian Mineralogist.

LE VAILLANT, M., BARNES, S.J., FIORENTINI, M.L., BARNES, S.-J., BATH, A. & MILLER, J. (2018) Platinum-group element and gold contents of arsenide and sulfarsenide minerals associated with Ni and Au deposits in Archean greenstone belts. *Mineralogical Magazine* **82**, 625-647, 10.1180/minmag.2017.081.100.

LOCMELIS, M., MELCHER, F. & OBERTHÜR, T. (2010) Platinum-group element distribution in the oxidized Main Sulfide Zone, Great Dyke, Zimbabwe. *Mineralium Deposita* **45**, 93-109, 10.1007/s00126-009-0258-y.

LOCMELIS, M., PEARSON, N.J., BARNES, S.J. & FIORENTINI, M.L. (2011) Ruthenium in komatiitic chromite. *Geochimica et Cosmochimica Acta* **75**, 3645-3661, https://doi.org/10.1016/j.gca.2011.03.041.

LOCMELIS, M., FIORENTINI, M.L., BARNES, S.J. & PEARSON, N.J. (2013) Ruthenium variation in chromite from komatiites and komatiitic basalts - a potential mineralogical indicator for nickel sulfide mineralization. *Economic Geology* **108**, 355-364, https://doi.org/10.2113/econgeo.108.2.355.

LOCMELIS, M., FIORENTINI, M.L., BARNES, S.J., HANSKI, E.J. & KOBUSSEN, A.F. (2018) Ruthenium in chromite as indicator for magmatic sulfide liquid equilibration in mafic-ultramafic systems. *Ore Geology Reviews* **97**, 152-170, https://doi.org/10.1016/j.oregeorev.2018.05.002.

LOCMELIS, M., AREVALO, R.D., JR., PUCHTEL, I.S., FIORENTINI, M.L. & NISBET, E.G. (2019) Transition metals in komatiitic olivine: Proxies for mantle composition, redox conditions, and sulfide mineralization potential. *American Mineralogist* **104**, 1143-1155, https://doi.org/10.2138/am-2019-6914.

MAIER, W.D., BARNES, S.J., CAMPBELL, I.H., FIORENTINI, M.L., PELTONEN, P., BARNES, S.-J. & SMITHIES, R.H. (2009) Progressive mixing of meteoritic veneer into the early Earth's deep mantle. *Nature* **460**, 620-623, 10.1038/nature08205.

NALDRETT, A.J., KINNAIRD, J., WILSON, A., YUDOVSKAYA, M., MCQUADE, S., CHUNNETT, G. & STANLEY, C. (2009a) Chromite composition and PGE content of Bushveld chromitites: Part 1 – the Lower and Middle Groups. *Applied Earth Science* **118**, 131-161, https://doi.org/10.1179/174327509X12550990458004.

NALDRETT, A.J., WILSON, A., KINNAIRD, J. & CHUNNETT, G. (2009b) PGE Tenor and Metal Ratios within and below the Merensky Reef, Bushveld Complex: Implications for its Genesis. *Journal of Petrology* **50**, 625-659, 10.1093/petrology/egp015.

NICKLAS, R.W., PUCHTEL, I.S., ASH, R.D., PICCOLI, P.M., HANSKI, E., NISBET, E.G., WATERTON, P., PEARSON, D.G. & ANBAR, A.D. (2019) Secular mantle oxidation across the Archean-Proterozoic boundary: Evidence from V partitioning in komatiites and picrites. *Geochimica et Cosmochimica Acta* **250**, 49-75, https://doi.org/10.1016/j.gca.2019.01.037.

NORMAN, M.D., PEARSON, N.J., SHARMA, A. & GRIFFIN, W.L. (1996) Quantitative analysis of trace elements in geological materials by laser ablation ICPMS: instrumental operating conditions and calibration values of NIST glasses. **20**, 247-261, https://doi.org/10.1111/j.1751-908X.1996.tb00186.x.

OCCHIPINTI, S.A., SHEPPARD, S., PASSCHIER, C., TYLER, I.M. & NELSON, D.R. (2004) Palaeoproterozoic crustal accretion and collision in the southern Capricorn Orogen: the Glenburgh Orogeny. *Precambrian Research* **128**, 237-255, https://doi.org/10.1016/j.precamres.2003.09.002.

PAGÉ, P., BARNES, S.-J., BÉDARD, J.H. & ZIENTEK, M.L. (2012) In situ determination of Os, Ir, and Ru in chromites formed from komatiite, tholeiite and boninite magmas: Implications for chromite control of Os, Ir and Ru during partial melting and crystal fractionation. *Chemical Geology* **302**, 3-15, https://doi.org/10.1016/j.chemgeo.2011.06.006.

PAGÉ, P. & BARNES, S.-J. (2016) The influence of chromite on osmium, iridium, ruthenium and rhodium distribution during early magmatic processes. *Chemical Geology* **420**, 51-68, https://doi.org/10.1016/j.chemgeo.2015.11.002.

PAGÉ, P. & BARNES, S.-J. (2009) Using Trace Elements in Chromites to Constrain the Origin of Podiform Chromitites in the Thetford Mines Ophiolite, Québec, Canada. *Economic Geology* **104**, 997-1018, https://doi.org/10.2113/econgeo.104.7.997.

PARK, J.-W., CAMPBELL, I.H. & EGGINS, S.M. (2012) Enrichment of Rh, Ru, Ir and Os in Cr spinels from oxidized magmas: Evidence from the Ambae volcano, Vanuatu. *Geochimica et Cosmochimica Acta* **78**, 28-50, http://dx.doi.org/10.1016/j.gca.2011.11.018.

PARK, J.-W., KAMENETSKY, V., CAMPBELL, I., PARK, G., HANSKI, E. & PUSHKAREV, E. (2017) Empirical constraints on partitioning of platinum group elements between Cr-spinel and primitive terrestrial magmas. *Geochimica et Cosmochimica Acta* **216**, 393-416, https://doi.org/10.1016/j.gca.2017.05.039.

PATON, C., HELLSTROM, J., PAUL, B., WOODHEAD, J. & HERGT, J. (2011) Iolite: Freeware for the visualisation and processing of mass spectrometric data. *Journal of Analytical Atomic Spectrometry* **26**, 2508-2518, https://doi.org/10.1039/C1JA10172B.

PRICHARD, H.M., J., B.S., DALE, C.W., GODEL, B., FISHER, P.C. & NOWELL, G.M. (2017) Paragenesis of multiple platinum-group mineral populations in Shetland ophiolite chromitite: 3D X-ray tomography and in situ Os isotopes. *Geochimica et Cosmochimica Acta* **216**, 314-334, http://dx.doi.org/10.1016/j.gca.2017.03.035.

PUCHTEL, I.S., HUMAYUN, M., CAMPBELL, A.J., SPROULE, R.A. & LESHER, C.M. (2004) Platinum group element geochemistry of komatiites from the Alexo and Pyke Hill areas, Ontario, Canada 11Associate editor: R. J. Walker. *Geochimica et Cosmochimica Acta* **68**, 1361-1383, https://doi.org/10.1016/j.gca.2003.09.013.

PUCHTEL, I.S. & HUMAYUN, M. (2005) Highly siderophile element geochemistry of 187Os-enriched 2.8 Ga Kostomuksha komatiites, Baltic Shield. *Geochimica et Cosmochimica Acta* **69**, 1607-1618, https://doi.org/10.1016/j.gca.2004.09.007.

PUCHTEL, I.S., HUMAYUN, M. & WALKER, R.J. (2007) Os–Pb–Nd isotope and highly siderophile and lithophile trace element systematics of komatiitic rocks from the Volotsk suite, SE Baltic Shield. *Precambrian Research* **158**, 119-137, https://doi.org/10.1016/j.precamres.2007.04.004.

PUCHTEL, I.S., WALKER, R.J., ANHAEUSSER, C.R. & GRUAU, G. (2009a) Re–Os isotope systematics and HSE abundances of the 3.5 Ga Schapenburg komatiites, South Africa: Hydrous melting or prolonged survival of primordial heterogeneities in the mantle? *Chemical Geology* **262**, 355-369, https://doi.org/10.1016/j.chemgeo.2009.02.006.

PUCHTEL, I.S., WALKER, R.J., BRANDON, A.D. & NISBET, E.G. (2009b) Pt–Re–Os and Sm–Nd isotope and HSE and REE systematics of the 2.7Ga Belingwe and Abitibi komatiites. *Geochimica et Cosmochimica Acta* **73**, 6367-6389, https://doi.org/10.1016/j.gca.2009.07.022.

PUCHTEL, I.S., WALKER, R.J., TOUBOUL, M., NISBET, E.G. & BYERLY, G.R. (2014) Insights into early Earth from the Pt–Re–Os isotope and highly siderophile element abundance systematics of Barberton komatiites. *Geochimica et Cosmochimica Acta* **125**, 394-413, https://doi.org/10.1016/j.gca.2013.10.013.

PUCHTEL, I.S., BLICHERT-TOFT, J., TOUBOUL, M., HORAN, M.F. & WALKER, R.J. (2016a) The coupled 182W-142Nd record of early terrestrial mantle differentiation. **17**, 2168-2193, https://doi.org/10.1002/2016GC006324.

PUCHTEL, I.S., TOUBOUL, M., BLICHERT-TOFT, J., WALKER, R.J., BRANDON, A.D., NICKLAS, R.W., KULIKOV, V.S. & SAMSONOV, A.V. (2016b) Lithophile and siderophile element systematics of Earth's mantle at the Archean–Proterozoic boundary: Evidence from 2.4Gakomatiites. *Geochimica et Cosmochimica Acta* **180**, 227-255, https://doi.org/10.1016/j.gca.2016.02.027.

PUCHTEL, I.S., BLICHERT-TOFT, J., TOUBOUL, M. & WALKER, R.J. (2018) 182W and HSE constraints from 2.7 Ga komatiites on the heterogeneous nature of the Archean mantle. *Geochimica et Cosmochimica Acta* **228**, 1-26, https://doi.org/10.1016/j.gca.2018.02.030.

PUCHTEL, I.S., MUNDL-PETERMEIER, A., HORAN, M., HANSKI, E.J., BLICHERT-TOFT, J. & WALKER, R.J. (2020) Ultra-depleted 2.05 Ga komatiites of Finnish Lapland: Products of grainy late accretion or core-mantle interaction? *Chemical Geology* **554**, 119801, https://doi.org/10.1016/j.chemgeo.2020.119801.

PUCHTEL, I.S., NICKLAS, R.W., SLAGLE, J., HORAN, M., WALKER, R.J., NISBET, E.G. & LOCMELIS, M. (2022) Early global mantle chemical and isotope heterogeneity revealed by the komatiite-basalt record: The Western Australia connection. *Geochimica et Cosmochimica Acta* **320**, 238-278, https://doi.org/10.1016/j.gca.2021.11.030.

REHKÄMPER, M. & HALLIDAY, A.N. (1997) Development and application of new iondashexchange techniques for the separation of the platinum group and other siderophile elements from geological samples. *Talanta* **44**, 663-672, https://doi.org/10.1016/S0039-9140(96)02100-5.

RIGHTER, K., CAMPBELL, A.J., HUMAYUN, M. & HERVIG, R.L. (2004) Partitioning of Ru, Rh, Pd, Re, Ir, and Au between Cr-bearing spinel, olivine, pyroxene and silicate melts. *Geochimica et Cosmochimica Acta* **68**, 867-880, https://doi.org/10.1016/j.gca.2003.07.005.

SCHINDELIN, J., ARGANDA-CARRERAS, I., FRISE, E., KAYNIG, V., LONGAIR, M., PIETZSCH, T., PREIBISCH, S., RUEDEN, C., SAALFELD, S., SCHMID, B., TINEVEZ, J.-Y., WHITE, D.J., HARTENSTEIN, V., ELICEIRI, K., TOMANCAK, P. & CARDONA, A. (2012) Fiji: an open-source platform for biological-image analysis. *Nature Methods* **9**, 676, 10.1038/nmeth.2019

https://www.nature.com/articles/nmeth.2019#supplementary-information.

SCHONEVELD, L., BARNES, S.J., MAKKONEN, H.V., LE VAILLANT, M., PATERSON, D.J., TARANOVIC, V., WANG, K.-Y. & MAO, Y.-J. (2020) Zoned Pyroxenes as Prospectivity Indicators for Magmatic Ni-Cu Sulfide Mineralization. *Frontiers in Earth Science* **8**, 10.3389/feart.2020.00256.

SHIREY, S.B. & WALKER, R.J. (1998) The Re-Os isotope system in cosmochemistry and high-temperature geochemistry. **26**, 423-500, https://doi.org/10.1146/annurev.earth.26.1.423.

SMITH, W., MAIER, W., BARNES, S., MOORHEAD, G., REID, D. & KARYKOWSKI, B. (2021) Element mapping the Merensky Reef of the Bushveld Complex. *Geoscience Frontiers* **12**, 101101, https://doi.org/10.1016/j.gsf.2020.11.001.

SMOLIAR, M.I., WALKER, R.J. & MORGAN, J.W. (1996) Re-Os Ages of Group IIA, IIIA, IVA, and IVB Iron Meteorites. **271**, 1099-1102, https://doi.org/10.1126/science.271.5252.1099.

TEIGLER, B. & EALES, H.V. (1993) Correlation between chromite composition and PGE mineralization in the Critical Zone of the western Bushveld Complex. *Mineralium Deposita* **28**, 291-302, 10.1007/BF02739368.

TYLER, I.M. (1991) *The geology of the Sylvania Inlier and the southeast Hamersley Basin*. East Perth, W.A : Geological Survey of Western Australia, East Perth, W.A.

WALKER, R.J., HORAN, M.F., MORGAN, J.W., BECKER, H., GROSSMAN, J.N. & RUBIN, A.E. (2002) Comparative 187Re-187Os systematics of chondrites: Implications regarding early solar system processes. *Geochimica et Cosmochimica Acta* **66**, 4187-4201, https://doi.org/10.1016/S0016-7037(02)01003-7.

WILLIAMS, I.R. & TYLER, I.M. (1991) Robertson, Western Australia.1:250,000 Geological Series, Explanatory Notes: Perth (1:250,000). Geological Survey of Western Australia.

WILLIAMS, M.J., SCHONEVELD, L., MAO, Y., KLUMP, J., GOSSES, J., DALTON, H., BATH, A. & BARNES, S. (2020) pyrolite: Python for geochemistry. *Journal of Open Source Software* **5**, 2314, https://doi.org/10.21105/joss.02314.

WINGATE, M.T.D., LU, Y. & JOHNSON, S.P. (2019a) 216542: metamonzogranite, Garden Well; Geochronology Record 1560. *Geological Survey of Western Australia*.

WINGATE, M.T.D., LU, Y. & JOHNSON, S.P. (2019b) 216598: metarhyolite, Cubana Well; Geochronology Record 1568. *Geological Survey of Western Australia*.

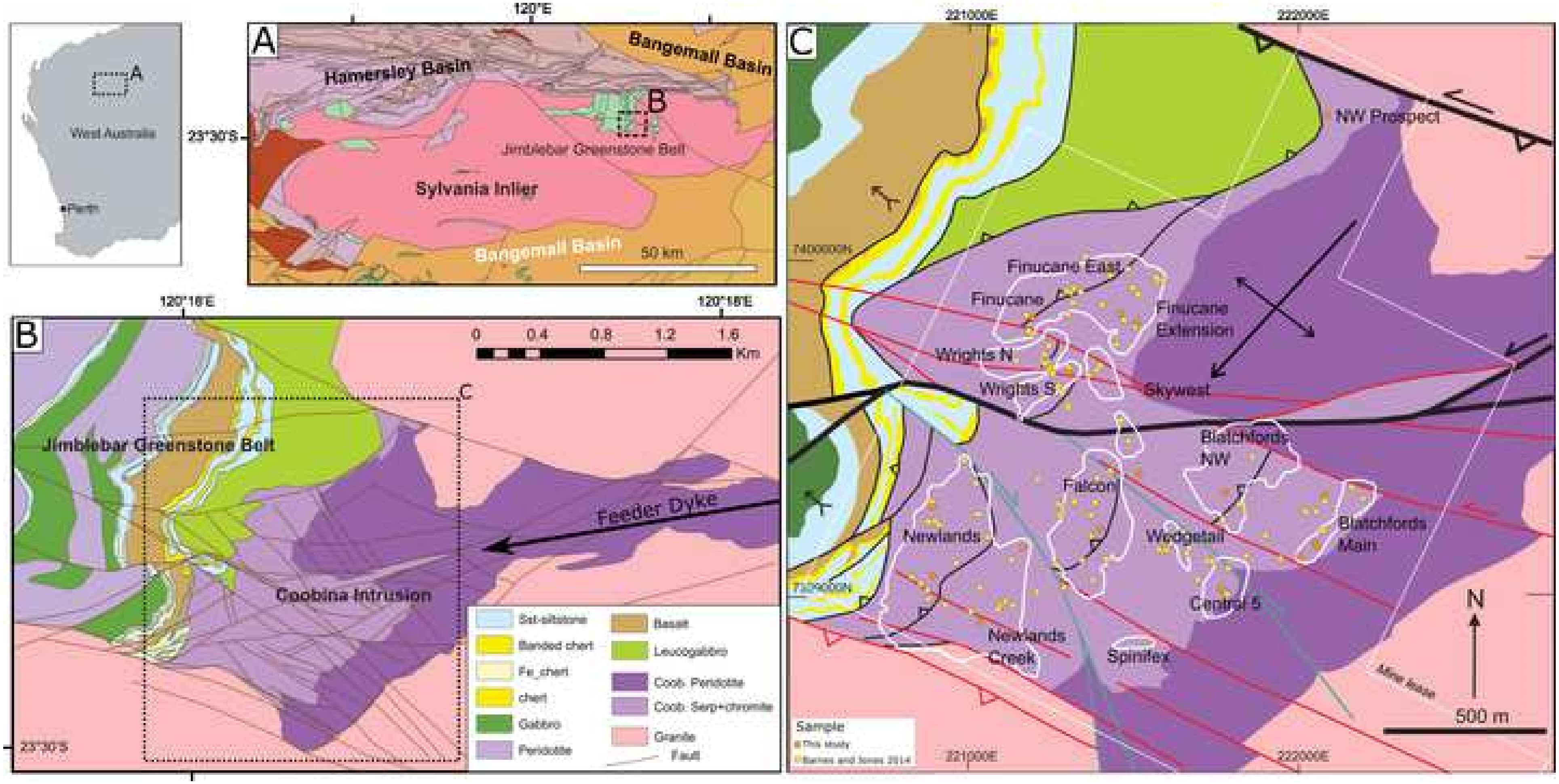
A
West Australia
Perth
120°E
23°30'S
A
Hamersley Basin
Bangemall Basin
B
Jimblebar Greenstone Belt
Sylvania Inlier
Bangemall Basin
50 km
120°16'E
120°18'E
B
0
0.4
0.8
1.2
1.6
Km
C
Jimblebar Greenstone Belt
Feeder Dyke
Coobina Intrusion
23°30'S
Sst-siltstone
Banded chert
Fe_chert
chert
Gabbro
Peridotite
Basalt
Leucogabbro
Coob. Peridotite
Coob. Serp+chromite
Granite
Fault
221000E
222000E
C
NW Prospect
7400000N
Finucane East
Finucane
Finucane Extension
Wrights N
Wrights S
Skywest
Blatchfords NW
Falcon
Newlands
Wedgetail
Blatchfords Main
7329000N
Central 5
Newlands Creek
Spinifex
Mine lease
N
500 m
Sample
This study
Barnes and Jones 2014
221000E
222000E

Figure2_outcrop

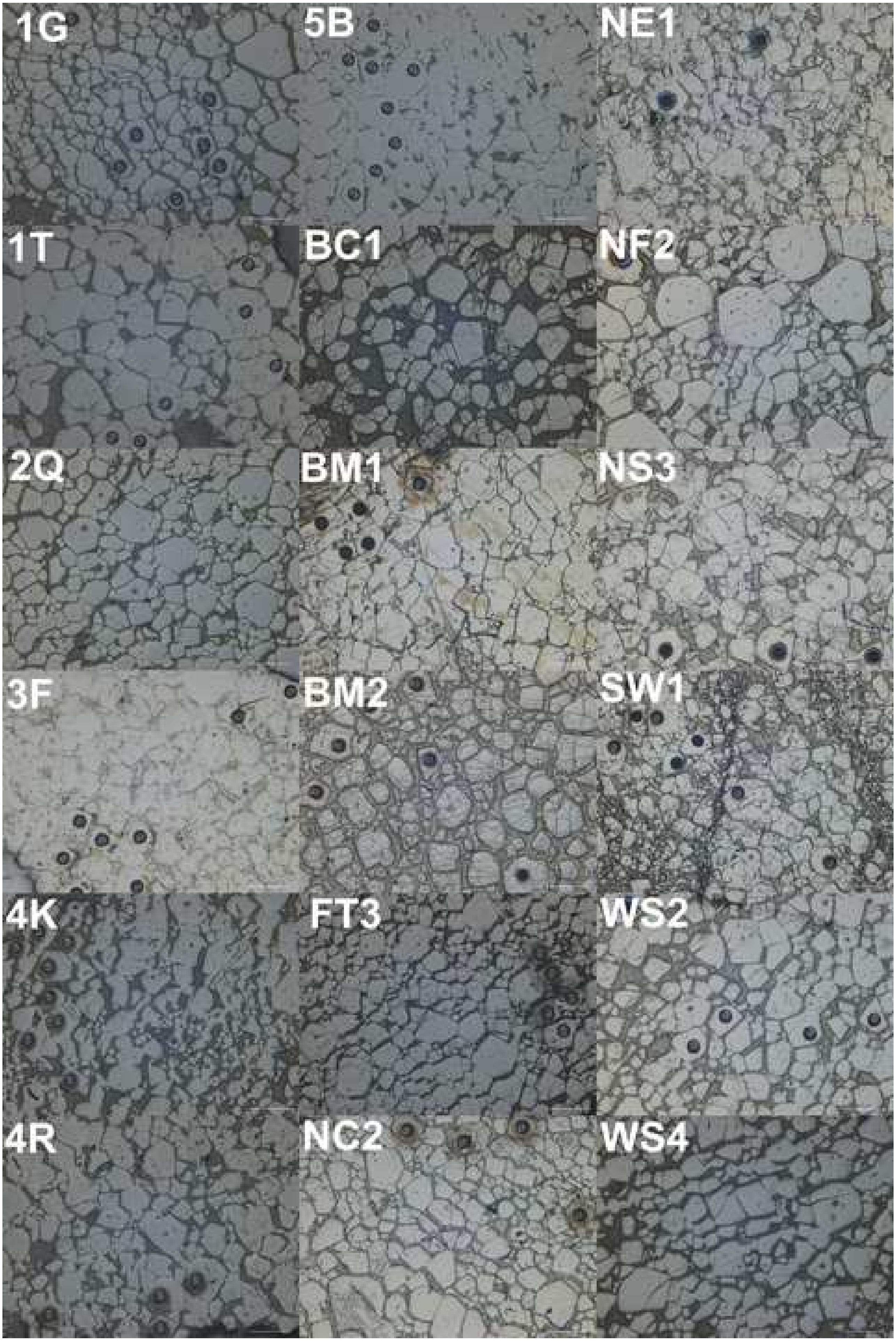
1G
5B
NE1
1T
BC1
NF2
2Q
BM1
NS3
3F
BM2
SW1
4K
FT3
WS2
4R
NC2
WS4

Figure4_CSD

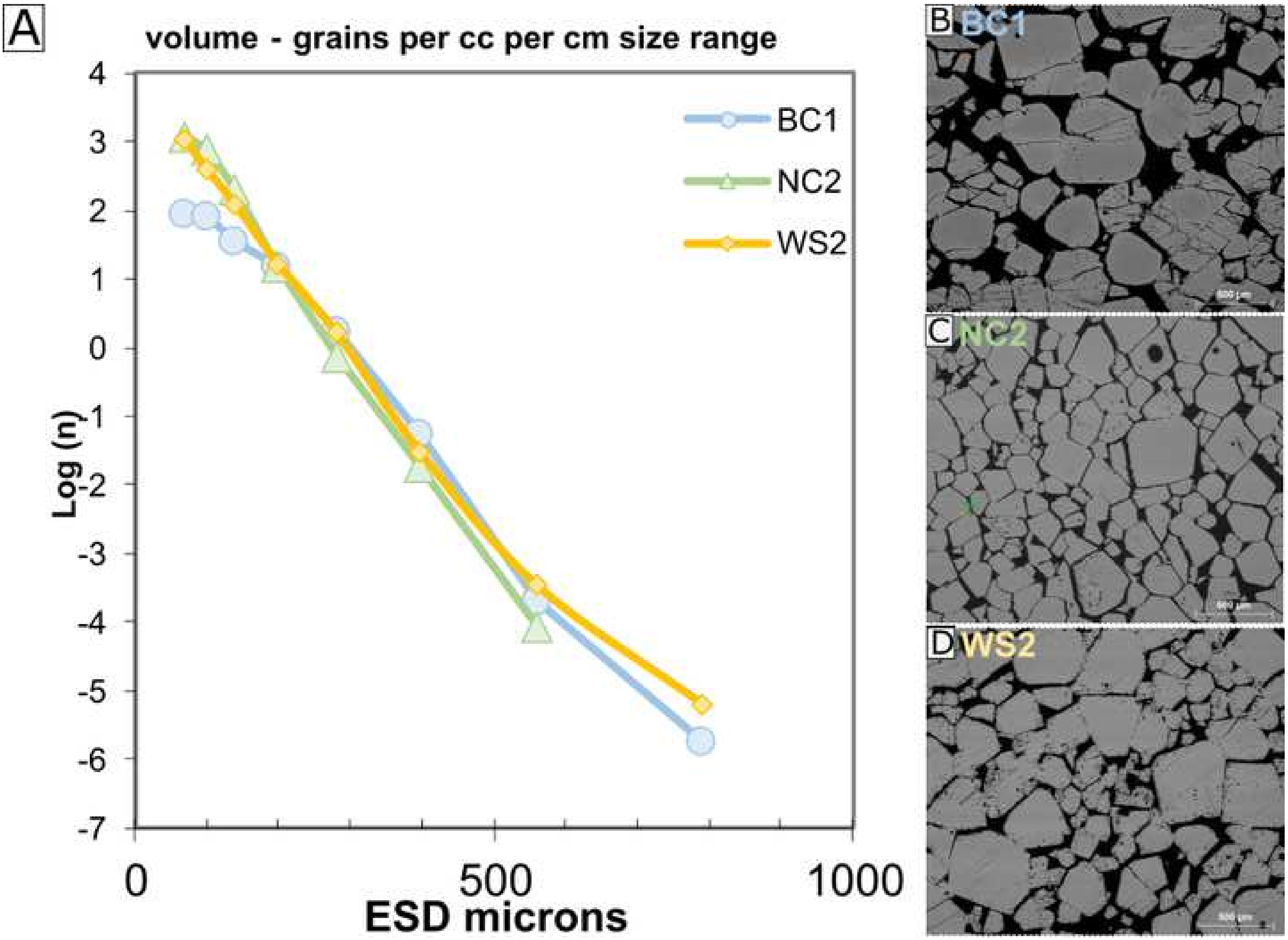
A
volume - grains per cc per cm size range
Log (n)
4
3
2
1
0
-1
-2
-3
-4
-5
-6
-7
0
500
1000
ESD microns
BC1
NC2
WS2
B BC1
C NC2
D WS2

Figure5_LiteratureData

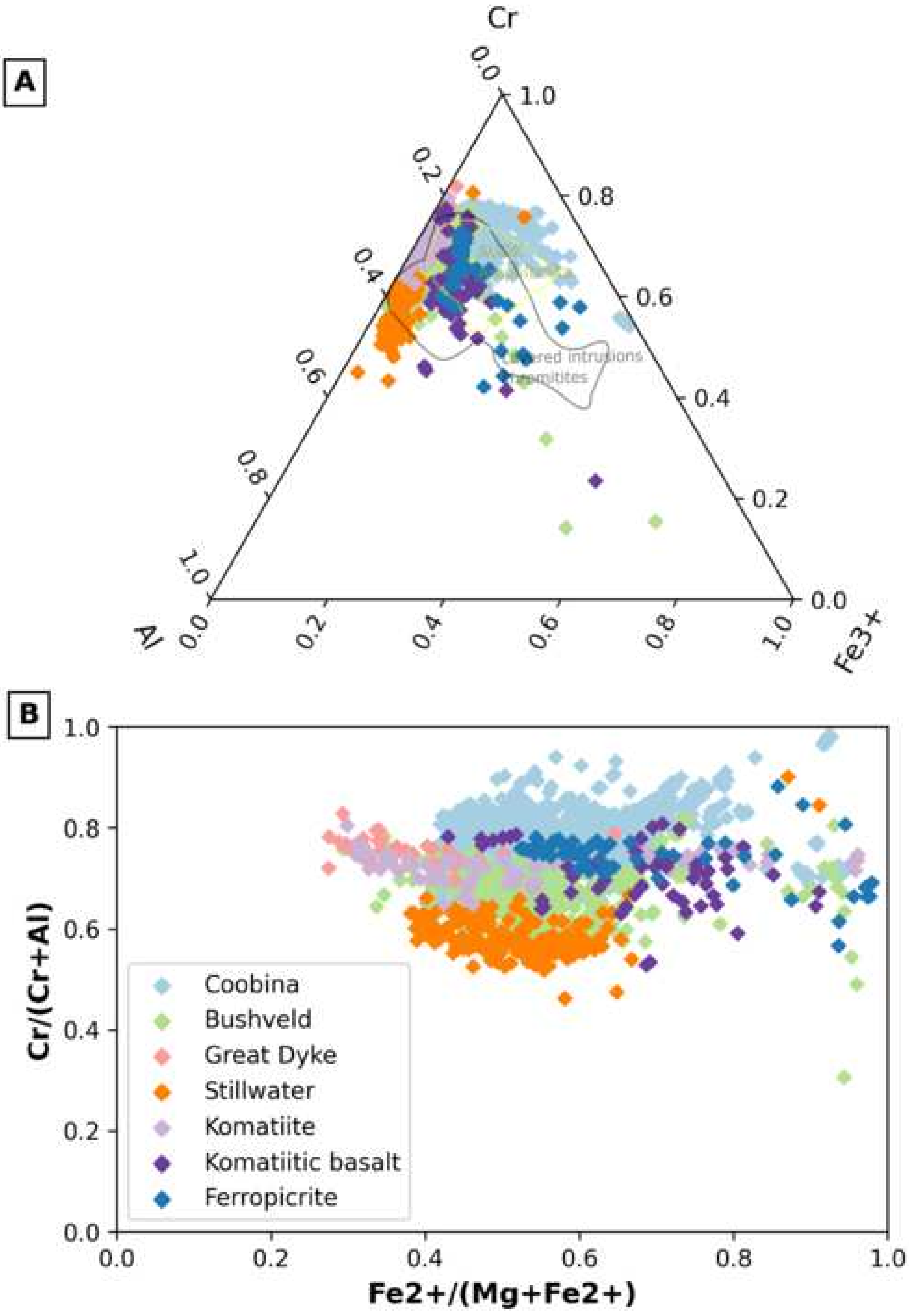

Figure6_TraceElements

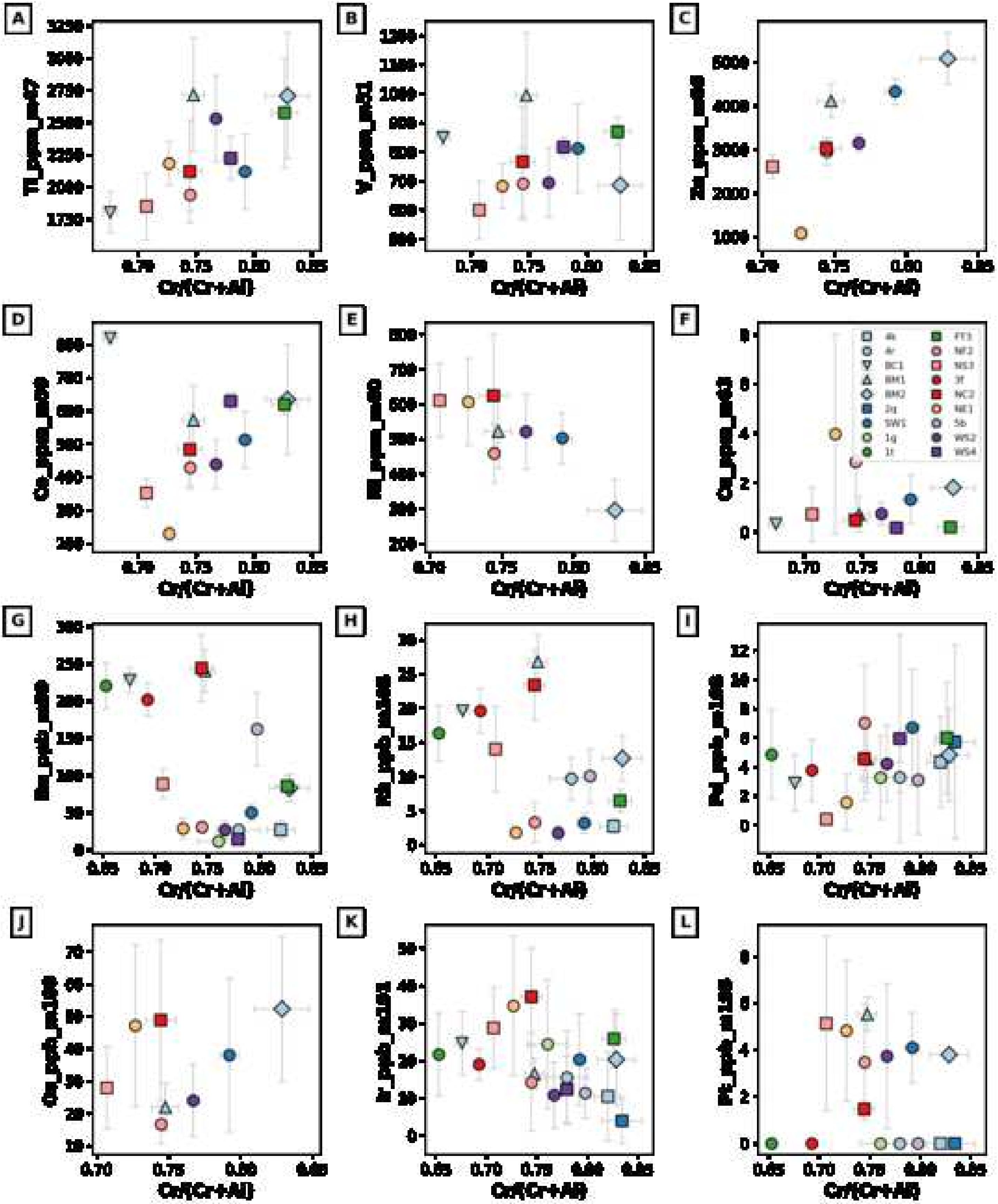

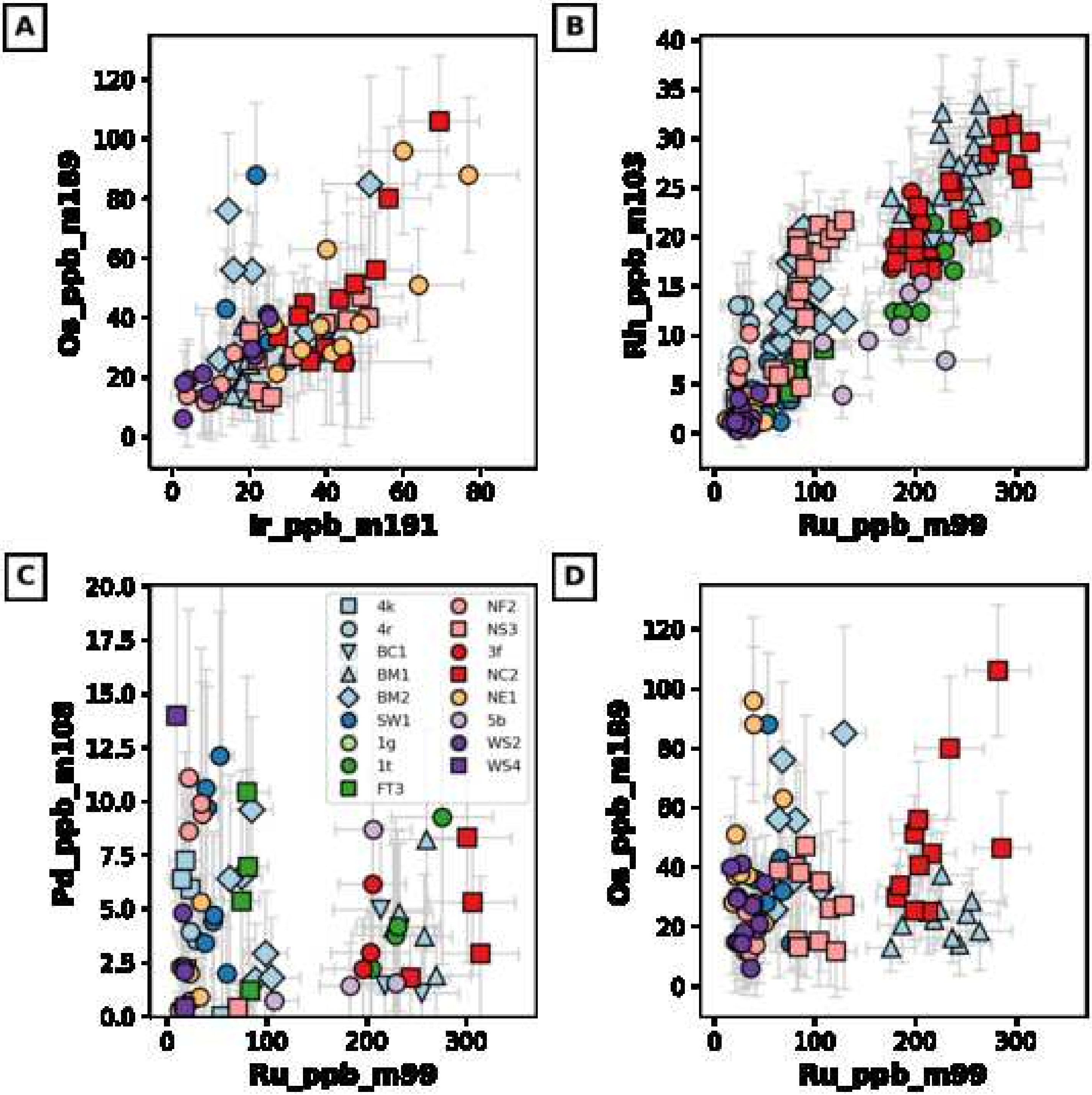
A
B
C
D
Os_ppb_m189
Ir_ppb_m191
0
20
40
60
80
100
120
Rh_ppb_m103
Ru_ppb_m99
0
5
10
15
20
25
30
35
40
100
200
300
Pd_ppb_m108
0.0
2.5
5.0
7.5
10.0
12.5
15.0
17.5
20.0
4k
4r
BC1
BM1
BM2
SW1
1g
1t
FT3
NF2
NS3
3f
NC2
NE1
5b
WS2
WS4

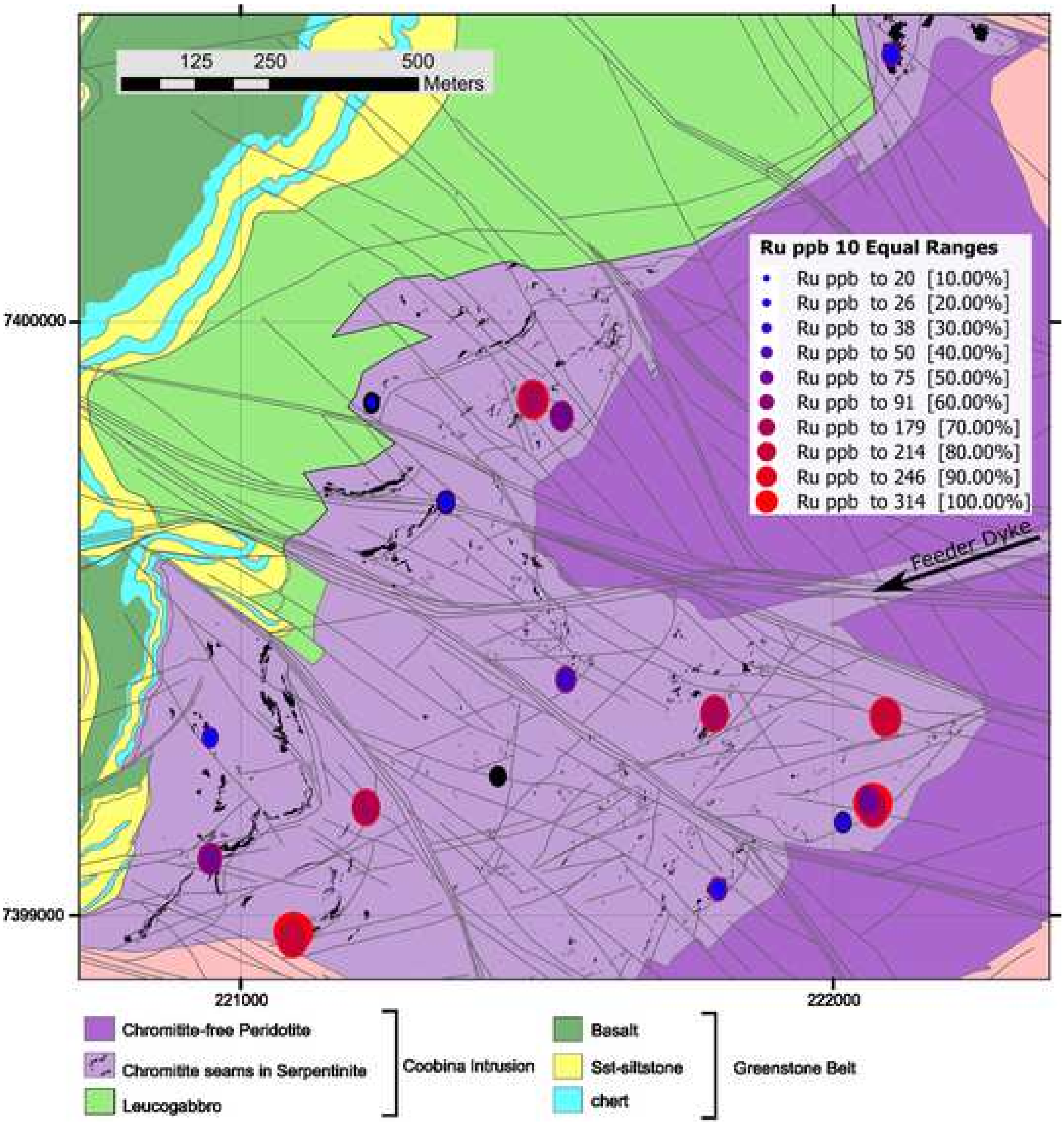
125
250
500
Meters
7400000
7399000
221000
222000
Ru ppb 10 Equal Ranges
Ru ppb to 20 [10.00%]
Ru ppb to 26 [20.00%]
Ru ppb to 38 [30.00%]
Ru ppb to 50 [40.00%]
Ru ppb to 75 [50.00%]
Ru ppb to 91 [60.00%]
Ru ppb to 179 [70.00%]
Ru ppb to 214 [80.00%]
Ru ppb to 246 [90.00%]
Ru ppb to 314 [100.00%]
Feeder Dyke
Chromitite-free Peridotite
Chromitite seams in Serpentinite
Leucogabbro
Coobina Intrusion
Basalt
Sst-siltstone
chert
Greenstone Belt

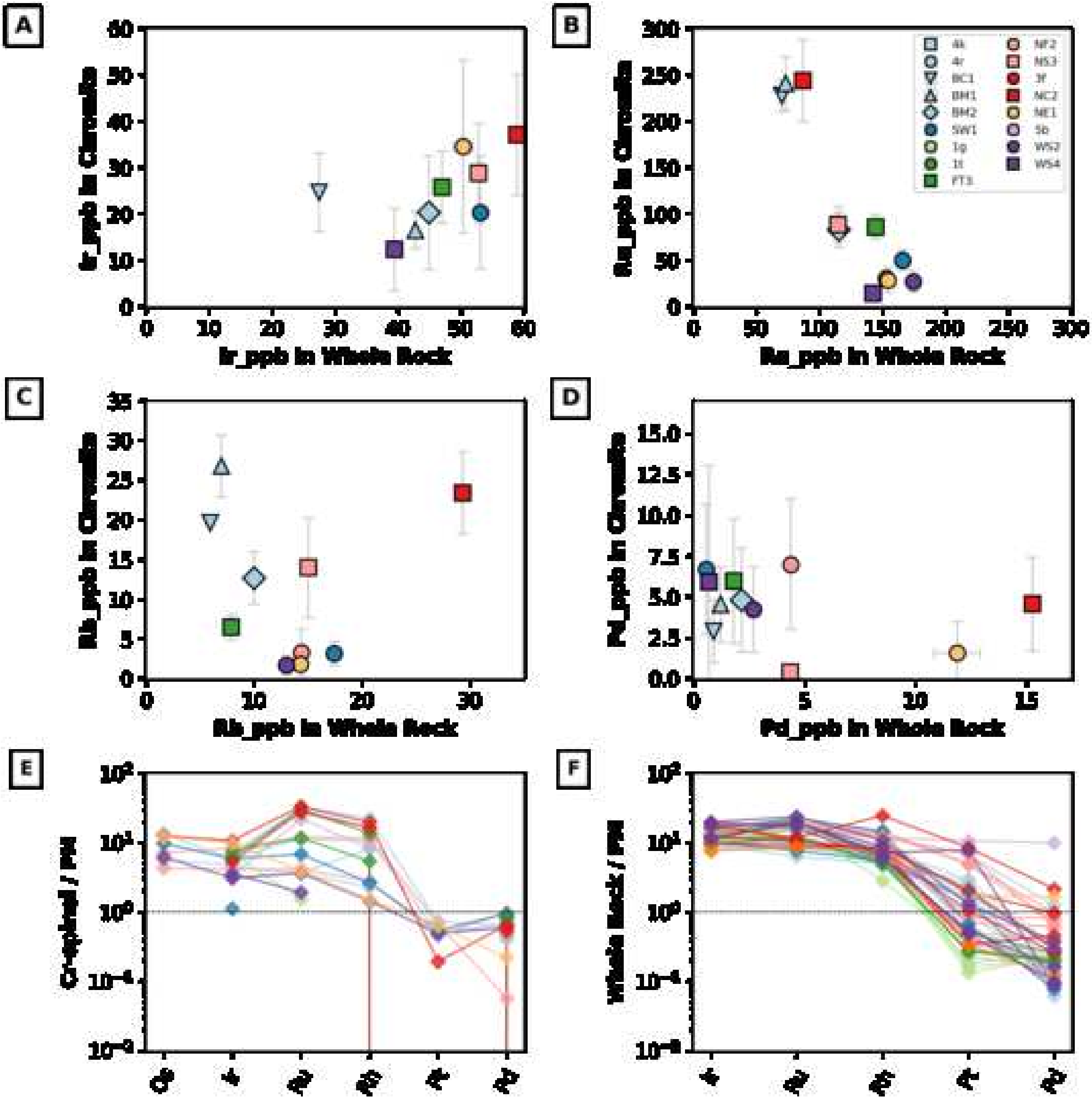
A
Ir_ppb in Chromite
Ir_ppb in Whole Rock
0
10
20
30
40
50
60
B
Ru_ppb in Chromite
Ru_ppb in Whole Rock
0
50
100
150
200
250
300
4k
4r
BC1
BM1
BM2
SW1
1g
1t
FT3
NF2
NS3
3f
NC2
NE1
5b
WS2
WS4
C
Rh_ppb in Chromite
Rh_ppb in Whole Rock
0
5
10
15
20
25
30
35
D
Pd_ppb in Chromite
Pd_ppb in Whole Rock
0.0
2.5
5.0
7.5
10.0
12.5
15.0
0
5
10
15
E
Cr-spinel / PM
10^2
10^1
10^0
10^{-1}
10^{-2}
Os
Ir
Ru
Rh
Pt
Pd
F
Whole Rock / PM
10^2
10^1
10^0
10^{-1}
10^{-2}
Ir
Ru
Rh
Pt
Pd

Figure 10.

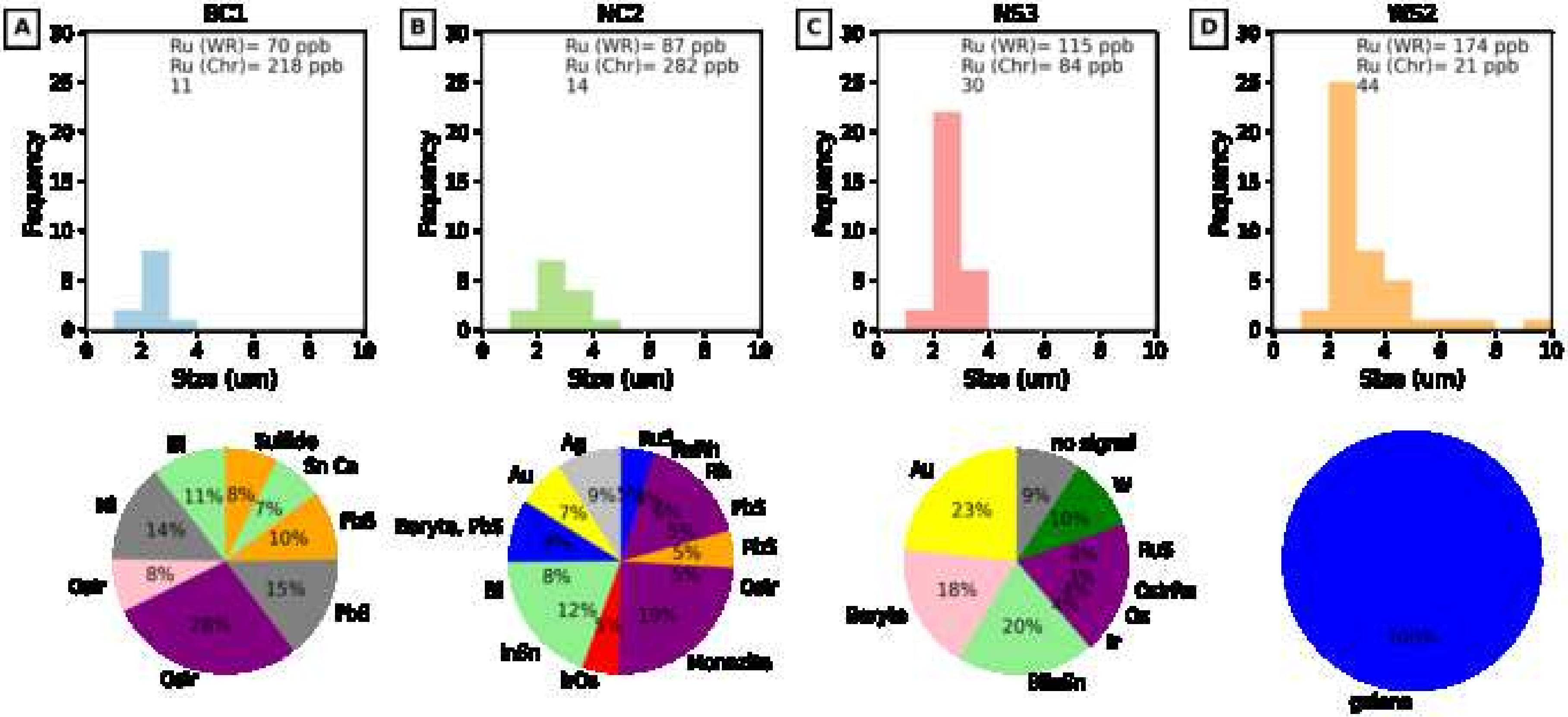
A
BC1
Ru (WR)= 70 ppb
Ru (Chr)= 218 ppb
11
B
NC2
Ru (WR)= 87 ppb
Ru (Chr)= 282 ppb
14
C
NS3
Ru (WR)= 115 ppb
Ru (Chr)= 84 ppb
30
D
WS2
Ru (WR)= 174 ppb
Ru (Chr)= 21 ppb
44
Frequency
0
5
10
15
20
25
30
Size (um)
0
2
4
6
8
10
Bi
Sulfide
Sn Cu
PbS
PbS
OsIr
OsIr
Ni
11%
8%
7%
10%
15%
28%
8%
14%
Ag
RuS
RuRh
Rh
PbS
PbS
OsIr
Monazite
IrOs
InSn
Bi
Baryte, PbS
Au
9%
5%
5%
5%
19%
12%
8%
7%
no signal
W
RuS
OsIrRu
Os
Ir
BiSn
Baryte
Au
9%
10%
20%
18%
23%
galena
100%

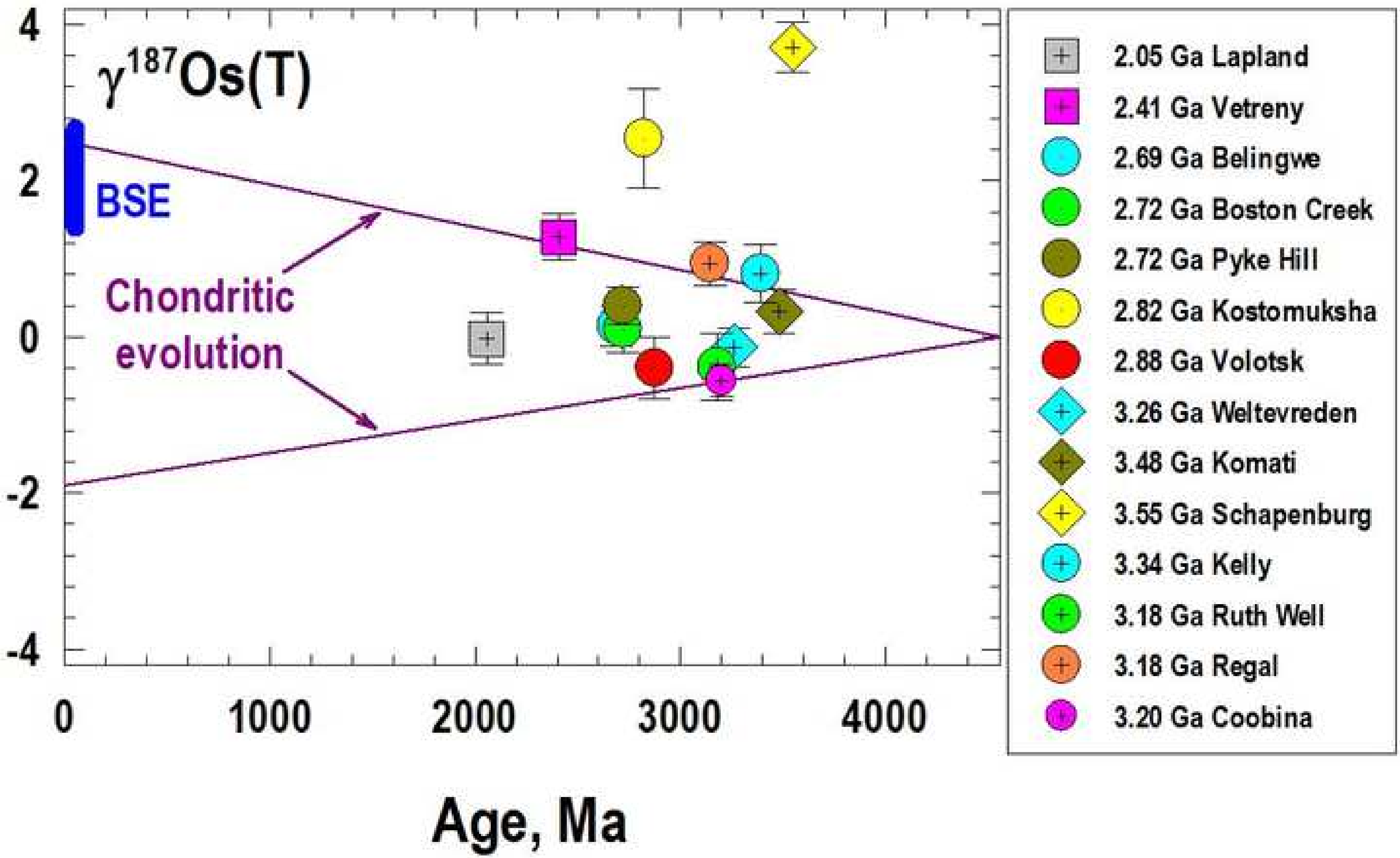
$\gamma^{187}Os(T)$
BSE
Chondritic evolution
4
2
0
-2
-4
0
1000
2000
3000
4000
Age, Ma
2.05 Ga Lapland
2.41 Ga Vetreny
2.69 Ga Belingwe
2.72 Ga Boston Creek
2.72 Ga Pyke Hill
2.82 Ga Kostomuksha
2.88 Ga Volotsk
3.26 Ga Weltevreden
3.48 Ga Komati
3.55 Ga Schapenburg
3.34 Ga Kelly
3.18 Ga Ruth Well
3.18 Ga Regal
3.20 Ga Coobina

Figure12_PGMs

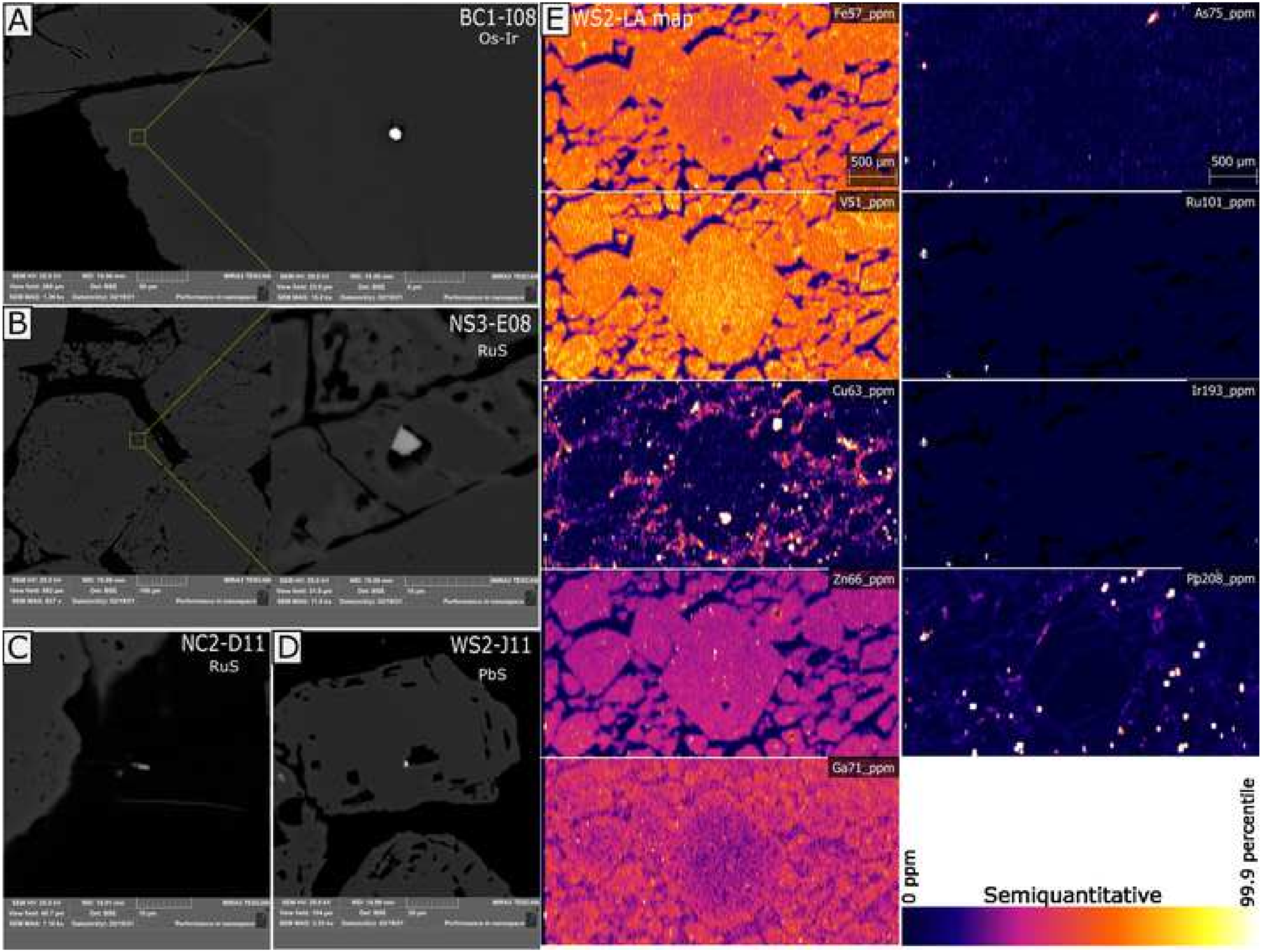

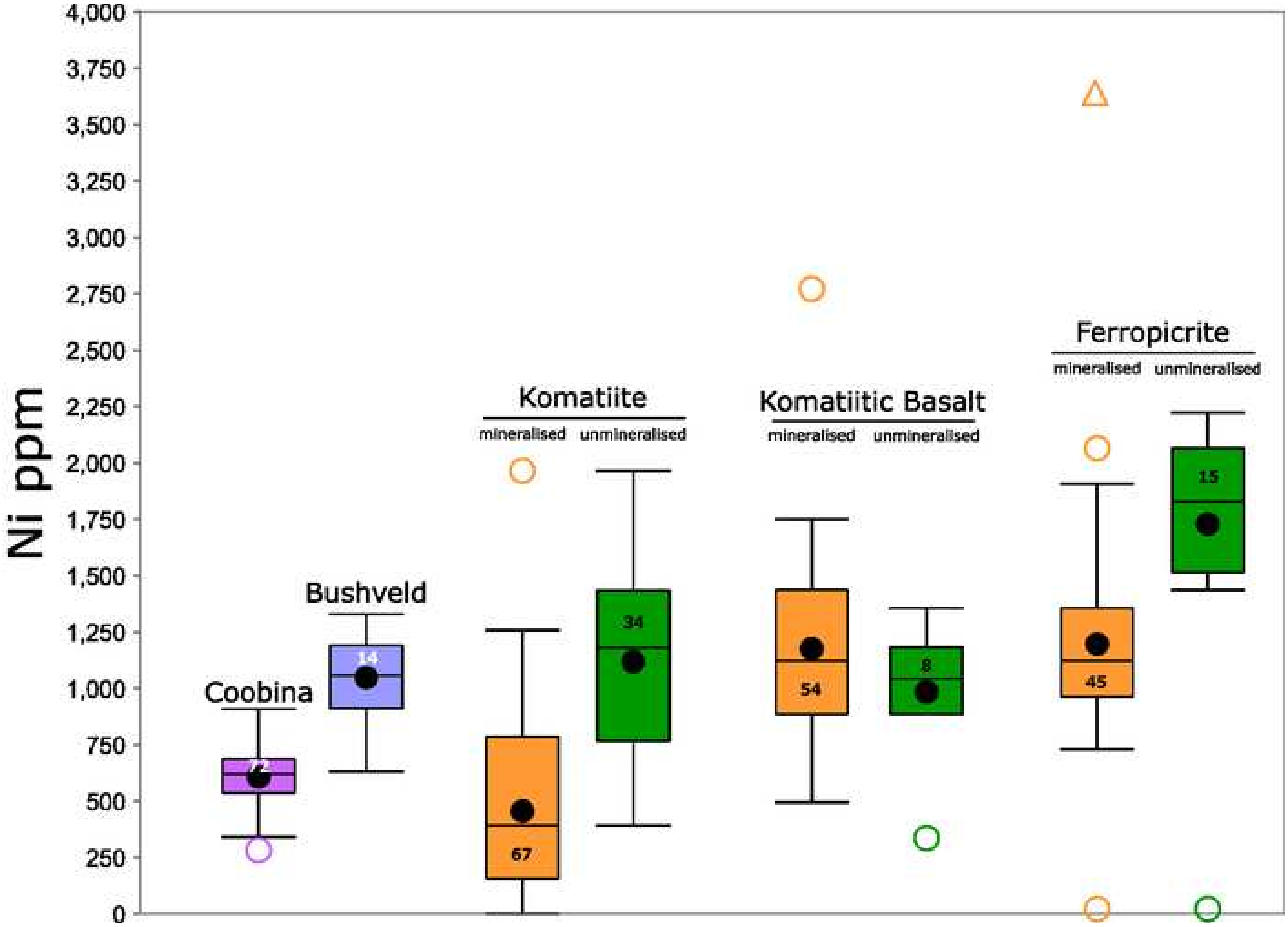
Ni ppm
4,000
3,750
3,500
3,250
3,000
2,750
2,500
2,250
2,000
1,750
1,500
1,250
1,000
750
500
250
0
Coobina
Bushveld
14
Komatiite
mineralised
unmineralised
67
34
Komatiitic Basalt
mineralised
unmineralised
54
8
Ferropicrite
mineralised
unmineralised
45
15

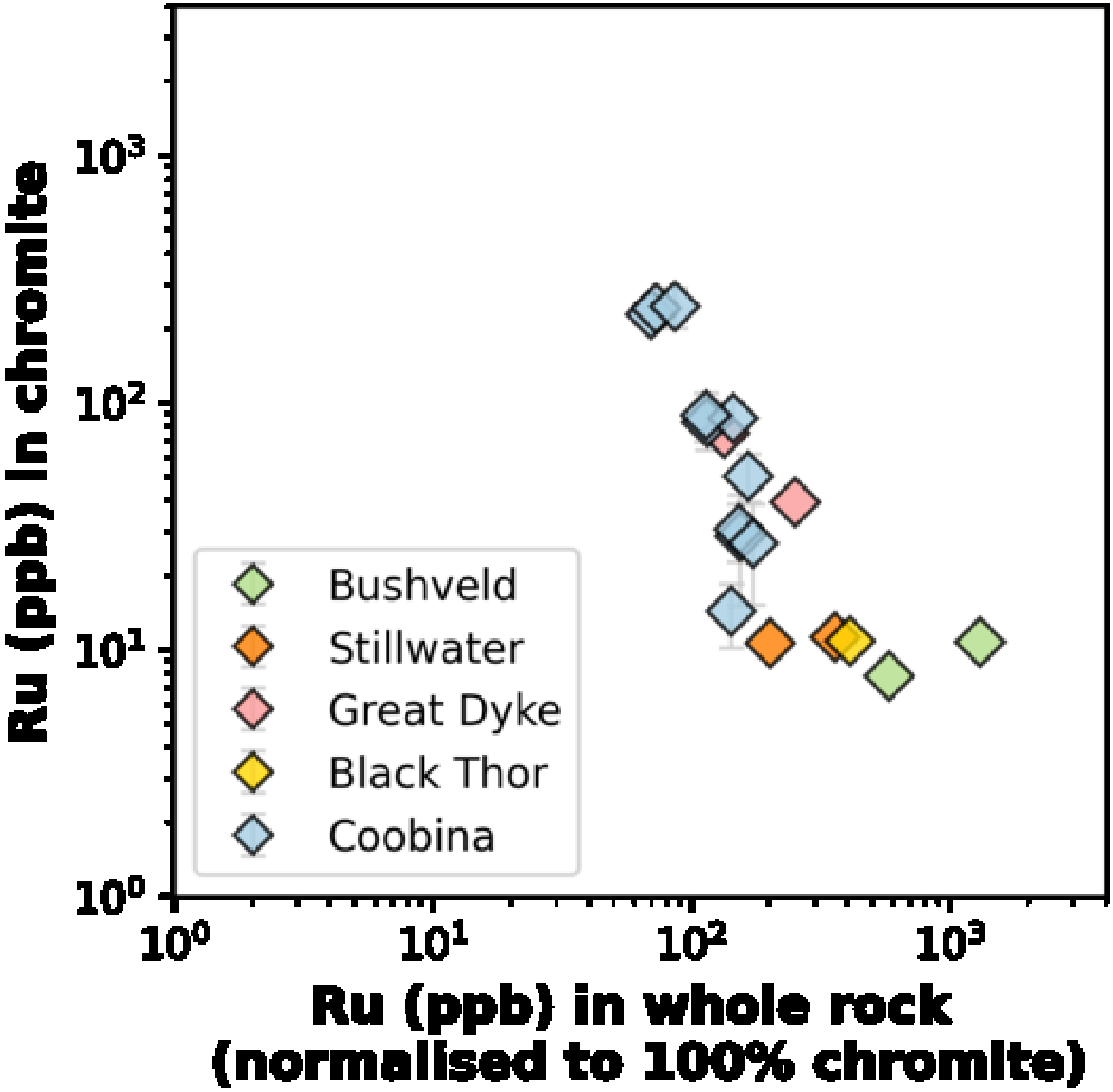
Ru (ppb) in chromite
Ru (ppb) in whole rock
(normalised to 100% chromite)
10^0
10^1
10^2
10^3
Bushveld
Stillwater
Great Dyke
Black Thor
Coobina